Four-Craft Virtual Coulomb Structure Analysis for 1 to 3 Dimensional Geometries

Harsh A. Vasavada

Thesis submitted to the Faculty of the
Virginia Polytechnic Institute and State University
in partial fulfillment of the requirements for the degree of

Master of Science
in
Aerospace Engineering

Hanspeter Schaub, Chair
Christopher D. Hall
Craig A. Woolsey

April 13, 2007
Blacksburg, Virginia

Keywords: Static Coulomb Formation, Distributed Genetic Algorithms

Four-Craft Virtual Coulomb Structure Analysis
for 1 to 3 Dimensional Geometries

Harsh A. Vasavada

(ABSTRACT)

Coulomb propulsion has been proposed for spacecraft cluster applications with separation distances on the order of dozens of meters. This thesis presents an investigation of analytic charge solutions for a planar and three dimensional four satellite formations. The solutions are formulated in terms of the formation geometry. In contrast to the two and three spacecraft Coulomb formations, a four spacecraft formation has additional constraints that need to be satisfied for the individual charges on the spacecraft to be unique and real. A spacecraft must not only satisfy the previously developed inequality constraints to yield a real charge solution, but it must also satisfy three additional equality constraints to ensure the spacecraft charge is unique. Further, a method is presented to reduce the number of equality constraints arising due the dynamics of a four spacecraft formation. Formation geometries are explored to determine the feasibility of orienting a square formation arbitrarily in any given plane. The unique and real spacecraft charges are determined as functions of the orientation of the square formation in a given principal orbit plane. For a three-dimensional tetrahedron formation, the charge products obtained are a unique set of solution. The full three-dimensional rotation of a tetrahedron is reduced to a two angle rotation for simpler analysis. The number of equality constraints for unique spacecraft charges can not be reduced for a three-dimensional formation. The two angle rotation results are presented for different values of the third angle. The thesis also presents the set up for a co-linear four-craft problem. The solution for the co-linear formation is not developed. The discussion of co-linear formations serves as an open question on how to determine analytic solutions for system with null-space dimension greater than 1. The thesis also presents a numerical tool for determining potential shapes of a static Coulomb formation as a support to the analytical solutions. The numerical strategy presented here uses a distributed Genetic Algorithm (GA) as an optimization tool. The GA offers several advantages over traditional gradient based optimization methods. Distributing the work of the GA over several processors reduces the computation time to arrive at a solution. The thesis discusses the implementation of a distributed GA used in the analysis of a static Coulomb formation. The thesis also addresses the challenges of implementation of a distributed GA on a computing cluster and presents candidate solutions.

Dedication

In the memory of unfortunate victims of the tragedy that occurred on Blacksburg campus of Virginia Tech on 4.16.07. This thesis is dedicated to Ryan "Stack" Clark, Emily Jane Hilscher, Mary Read, Henry Lee, Leslie Sherman, Reema Samaha, Maxine Turner, Jarrett Lane, Dr. Liviu Librescu, Dr. Kevin Granata, Juan Ortiz, Dr. G V Loganathan, Prof. Jaime Bishop, Matt La Porte, Brian Bluhm, Caitlin Hammaren, Daniel Perez Ceuva, Ross Alameddine, Erin Peterson, Julia Pryde, Mike Pohle, Matthew Gwaltney, Prof. Jocelyne Couture-Nowak, Nicole White, Dan O'Neil, Jeremy Herbstritt, Lauren McCain, Austin Cloyd, Rachael Hill, Parthi Lombantoruan, Waleed Shaalan and Minal Panchal. You may be out of sight, but never ever will you be out of mind.

Acknowledgments

I would like to thank Dr. Hanspeter Schaub for all the help and guidance he has provided over the course of my graduate studies. I would also like to thank him for financially supporting me and allowing me to work on an interesting project. I can never fully express my gratitude to Dr. Schaub, for without him this thesis would not be possible.

Contents

List of Figures

List of Tables

Chapter 1

Introduction

1.1 Virtual Coulomb Structure

Spacecraft formation or general proximity flying is increasingly gaining interest in the aerospace community. The benefits of a spacecraft formation include lower life cycle cost, reconfigurability of the formation shape and size, as well as adaptability of the formation in case of a malfunctioning satellite.[1,2,3,4] Applications such as synthetic aperture radar, space interferometry and sensor web formation are more feasible using spacecraft formation flying, rather than large monolithic structures.[1,2]

For small spacecraft separation distances on the order of 100 meters or less, thruster exhaust plume impingement issue with neighboring satellites is a major technological hurdle. Further, conventional chemical thrusting concepts are not effective in generating the small micro-Newton level forces required to maintain a cluster dozens of meters in size. Coulomb thrusting provides an attractive and novel solution to these technological hurdles arising from the control of a spacecraft in a tight formation.

The concept of Coulomb propulsion is based on the principles of electrostatic forces, which arise due to the interaction between two charged bodies. Spacecraft in the formation are charged to a certain potential. In the concept of static Coulomb formations the constant Coulomb forces are used to cancel out the relative motion dynamics and maintain a fixed formation with respect to the rotating formation chief Local Vertical/Local Horizontal(LVLH) frame. The electrostatic forces acting on the spacecraft are internal forces, and thus cannot change the total inertial angular momentum of the spacecraft.

Coulomb thrusting is considered an attractive solution as compared to electric propulsion for control of a spacecraft in a tight cluster of less than 100 meters. Electric propulsion is a fuel efficient method to control the spacecraft in a formation compared to traditional chemical thrusting concepts. The usefulness of electric propulsion is diminished for small separation distances between spacecraft, as the ionic exhaust plume could potentially damage near-by spacecraft. Coulomb propulsion has the advantage of being essentially propellant-less and offers mass savings up to 98%.[5,6] Coulomb propulsion is a highly efficient propulsion system achieving I_{sp} to the order of 10^{13}s. The power required to charge the spacecraft is in the order of watts (W).[6] In addition to being a highly efficient system, Coulomb propulsion is also based on a renewable source, increasing the mission lifetime as compared to electric propulsion.[7]

The concept of static Coulomb formation is similar to a virtual Coulomb structure. In a virtual Coulomb structure the truss and beam structural members are replaced with electrostatic force fields. In the presence of external disturbances, the force fields are only able to provide tension and compression to maintain the structural shape of a spacecraft cluster. The force fields maintain static virtual structures as seen by the rotating LVLH frame. Figure 1.1 shows a Coulomb virtual structure in space. Here the connections between spacecraft represent the electrostatic force fields acting on the spacecraft.

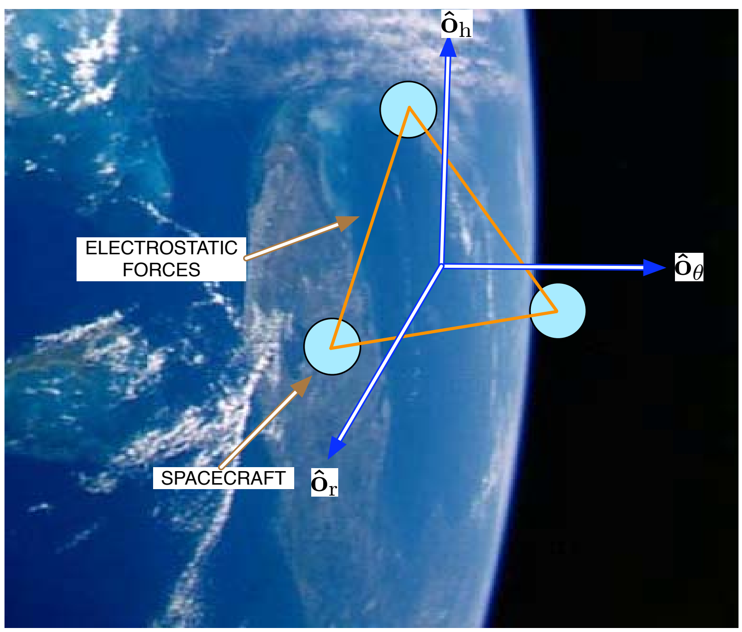

Figure 1.1: Coulomb virtual structure formation in space

This thesis presents analytical and numerical tools to find the open loop charges required to establish a static Coulomb formation. The charges required are held constant and there is no feedback to maintain the formation shape. The static formations are naturally occurring equilibrium solutions and the stability of such formations is not investigated in this thesis. Parker and King in the National Institute for Advanced Concepts (NIAC) report in Reference 5 present analytic solutions for three and five-craft formations. The analytic solutions presented in reference 5 used simplifying symmetry assumptions. Berryman and Schaub[7]

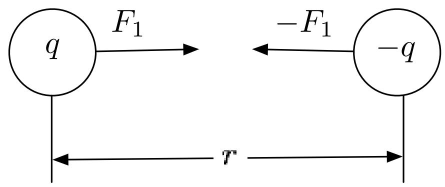

Figure 1.2: Interaction between two charged particles

present a more rigorous analysis for two and three-craft formations. The analytic solutions presented in this thesis build on the work done in References 5 and 7. This thesis presents the solutions for four-craft formations. The conditions required to determine unique and real spacecraft charges are presented in this thesis.

Analytic solutions for a square four-craft formation are presented. A square formation has practical applications for missions such as interferometry. The development of the work presented here assumes that the spacecraft have equal and constant masses. Analysis for a three-dimensional tetrahedron formation is also presented. The thesis also presents the set up of a one-dimensional four-craft formation.

1.2 Coulomb Thrusting Concept

The electrostatic Coulomb force between two charged bodies is proportional to the product of the charges and inversely proportional to the square of the distances between them, and the magnitude of this force is expressed as

$$F = k_c \frac{q_1 q_2}{r^2} e^{-\frac{r}{\lambda_d}} \tag{1.1}$$

Here $k_c = 8.988 \times 10^9$ Nm^{2}C^{-2} is the electrostatic constant and r the separation distance between spacecraft. Figure 1.2 illustrates the interaction between two equal but opposite charged particles. The exponential term in equation (1.1) represents the shielding effect of the space plasma environment through the term Debye length term λ_d. The plasma field in the space environment reduces the effect of Coulomb interaction by shielding the spacecraft. The Debye length in low Earth orbit is on the order of centimeters, thus requiring spacecraft to be charged to a large potential to overcome the plasma environment.[5,6] For the purposes of the analysis in this thesis, we assume the spacecraft clusters are in Geo-stationary Earth Orbit (GEO), where the Debye length ranges from 150m to 1000m making it more feasible to use Coulomb forces to control the formation.

Coulomb propulsion offers exciting potential applications for high Earth orbit missions such as rendezvous and proximity operations, and sparse aperture interferometry. Rendezvous and proximity operations involve using a micro-satellite for applications like space servicing, diagnostics and maintenance. Missions such as rendezvous and proximity operations involve small separation spacecraft distances on the order of a few dozen meters, making Coulomb control an attractive actuation mechanism. Figure 1.3 illustrates an example of sparse interferometry where the formation shape is controlled using electrostatic forces.

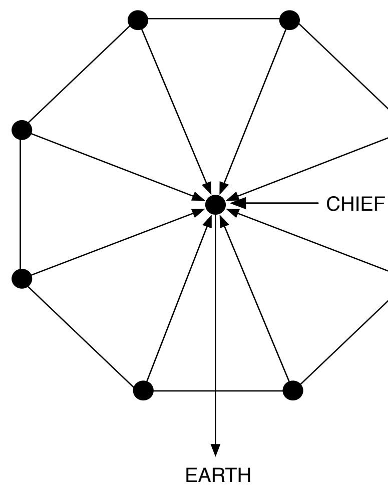

Figure 1.3: Sparse Interferometry using virtual Coulomb structure

1.3 Numerical Solutions

The interaction between Coulomb forces and the relative motion dynamics make determining the shape of potential formations non-intuitive. Thus there is a need for a numerical strategy to determine the possible shapes of the formations and the constant charges required on the spacecraft to implement a Coulomb formation. Typical gradient-based optimization techniques available require a good initial guess to the problem. Also the gradient-based methods restrict the search space to a local region around the initial guess.

Genetic Algorithms (GAs) are modern optimization tools that overcome the challenges arising from the use of gradient-based methods. GAs are based on the Darwinian principle of survival of the fittest, where the fittest members of a population survive and are allowed to reproduce. GAs have frequently been used to solve unconstrained problems such as optimal low thrust trajectories.[8] Krishna Kumar[9] presents an overview of GAs, outlining the steps involved in using a GA for an optimization problem. He also presents the use of Micro-GA and Fuzzy GA that are useful in certain kinds of optimization problems, and discusses the application of GA in aerospace optimization problems. Peng[10] discusses the use of a GA in control of inflatable structures. Here the GA is used to search for optimal tensions which minimize the membrane wrinkles.

The drawback of using a GA is the large amount of computation time required to arrive at a solution. The computation time can be reduced by distributing the work over several processors. This is achieved by dividing the overall population into smaller groups or sub-populations. This reduces the computation time required by each individual processor, thus reducing the overall computation time required for the optimization problem. Also, by allowing the migration among sub-populations, convergence to a local minimum can be avoided.[11]

Berryman and Schaub[12] present the use of GA's to numerically solve for positions and charges required in a static formation. Reference 5 presents numerical solutions for a six spacecraft formation. With use of GA's, numerical solutions for higher number of spacecraft formations can be determined as shown in Reference 12. Pettazzi et.al[13] discuss the use of a differential evolution algorithm (EA) to search for spacecraft charges in the Coulomb structure. The differential EA strategy presented in Reference 13 only searches for spacecraft charges, as the shape of the Coulomb structure is pre-set. The GA analysis presented in the thesis searches not only for spacecraft charges but also for the formation shape for a Coulomb structure to exist.

The thesis extends the work done by Berryman and Schaub[12] and presents the use of a distributed GA as a tool for determining the charges and the position of a spacecraft in a static formation. The thesis also explores the common problems, such as load balancing and exit criteria, typically associated with a parallel processing problem.

1.4 Literature Review

Parker and King performed the initial study on Coulomb thrusting in a NIAC Phase I project documented in reference 5. The NIAC report discusses Coulomb thrusting, potential applications, and simple techniques to find the static formation solutions using symmetry arguments. The report presents analytic solutions for three and five-craft formations and numerical solutions for a six spacecraft formation. The report uses simplifying assumptions based on symmetry, of the formation to determine the analytic solutions for charges on a spacecraft.

One of the challenging and interesting applications of Coulomb propulsion discussed in Reference 5 is the concept of a static Coulomb formation. The Coulomb forces exactly cancel out the relative motion dynamics creating a virtual Coulomb structure.[7,14] Berryman and Schaub[7] extend the work of Reference 5 and present a more rigorous analytic solutions for 2 and 3 spacecraft formations.

The necessary equilibrium conditions for static Coulomb formations with constant charges are developed in Reference 15. The conditions require that the center of mass of the static formation structure should be at the origin of the LVLH frame. Also the formation principal inertia axes of the static formation structure need to be aligned with the LVLH frame axes.

Natarajan and Schaub[14] present the 2-craft Coulomb tether structure concept. Here an electrostatic force field replaces the physical tether. The paper also presents the use of the gravity-gradient torque to stabilize the virtual Coulomb structure about the orbit nadir direction. Reference 14 discusses the first feedback law for a stabilized virtual Coulomb structure, with the separation distance and time rate change of separation distance as feedback terms.

References 16 and 17 develop control laws to maintain a charged spacecraft cluster. Reference 16 develops a control strategy to control a 2-satellite Coulomb formation. Reference 16 develops a non-linear control law based on orbit element differences, and proves the stability of such a law. Reference 17 discusses the potential use of electrostatic Coulomb forces for spacecraft collision avoidance using separation distance as feedback. Another exciting application of Coulomb propulsion is given by Pettazzi et.al in Reference 18. Here the hybrid use of electrostatic forces and conventional thrusting for swarm navigation and reconfiguration is discussed. The paper also discusses the different strategies for integrating the Coulomb actuation into swarm navigation and reconfiguration scheme. Application of Coulomb forces in aiding the self-assembly of the large space structures is discussed in Reference 19. These references illustrate the potential uses of Coulomb forces in aerospace applications. The references also demonstrate the novelty and viability of the concept of Coulomb thrusting.

The use of interacting force fields to control the spacecraft in a formation extends beyond Coulomb forces. There have been several instances where electromagnetic or Lorentz forces are proposed to control the spacecraft in a formation. Lorentz forces arise due to the motion of a charged particle in a magnetic field. Peck[20] presents the use of the Lorentz force as means for orbit control of small spacecraft. He also discusses the application of this technology in inclination control, Earth escape, nodal precession control and new sun-synchronous orbits. However, the required charge levels for Lorentz augmented orbits is several orders of magnitude larger than those proposed for the Coulomb thrusting concepts.

Atchison et.al in reference 21 presents the use of Lorentz force as means of propellant-less propulsion for capture into Jupiter's orbit. Reference 22 discusses the dynamics and control of electromagnetic satellite formations in Low Earth Orbits (LEO). Here the magnetic dipole is created by use of High Temperature Superconducting (HTS) wires. Kong et.al in reference 23 use electromagnetic forces to control multi-spacecraft arrays. In this paper electromagnetic dipoles in conjunction with reaction wheels are used on each spacecraft to control the inertial motion.

Chapter 2

Charged Spacecraft Equations of Motion

Let us define the rotating Hill frame coordinate system $\mathcal{H}$ in which the relative motion dynamics of the spacecraft formation will be expressed. The Hill frame is defined as $\mathcal{H} = \{O, \hat{o}_r, \hat{o}_\theta, \hat{o}_h\}$ as illustrated in figure 2. Here the orgin of the Hill frame lies at the center of mass of the formation. The vector $\hat{\mathbf{o}}_r$ points radially outward, $\hat{\mathbf{o}}_h$ points in the out of plane direction, and $\hat{\mathbf{o}}_\theta$ completes the coordinate system such that $\hat{\mathbf{o}}_\theta = \hat{\mathbf{o}}_h \times \hat{\mathbf{o}}_r$. The relative position vector between the deputy and the chief in inertial frame is expressed as $\boldsymbol{\rho_i} = \mathbf{r}_{d_i} - \mathbf{r}_c$, where $\mathbf{r}_{d_i}$ is the inertial position of the deputy spacecraft and $\mathbf{r}_c$ is the inertial position of the chief satellite. The relative position vector in Hill frame components is expressed as

$$
{}^{\mathcal{H}}\boldsymbol{\rho_i} = \left\{ \begin{array}{c} x_i \\ y_i \\ z_i \end{array} \right\} \tag{2.1}
$$

For a circular chief orbit, and for small spacecraft separation distance, the relative motion differential equation of the deputy is expressed as follows[24,25,26]

$$
\begin{aligned}
\ddot{x}_i - 2n\dot{y}_i - 3n^2 x_i &= A_{\mathrm{x}} && \text{(2.2a)}\\
\ddot{y}_i + 2n\dot{x}_i &= A_{\mathrm{y}} && \text{(2.2b)}\\
\ddot{z}_i + n^2 z_i &= A_{\mathrm{z}} && \text{(2.2c)}
\end{aligned}
$$

here n is the mean orbit rate of the chief.

The conditions for a Coulomb formation are achieved by allowing the electrostatic forces to cancel out the relative acceleration experienced in the Hill frame. Using the definition of electrostatic force given in (1.1) the linearized charged relative equations of motion are

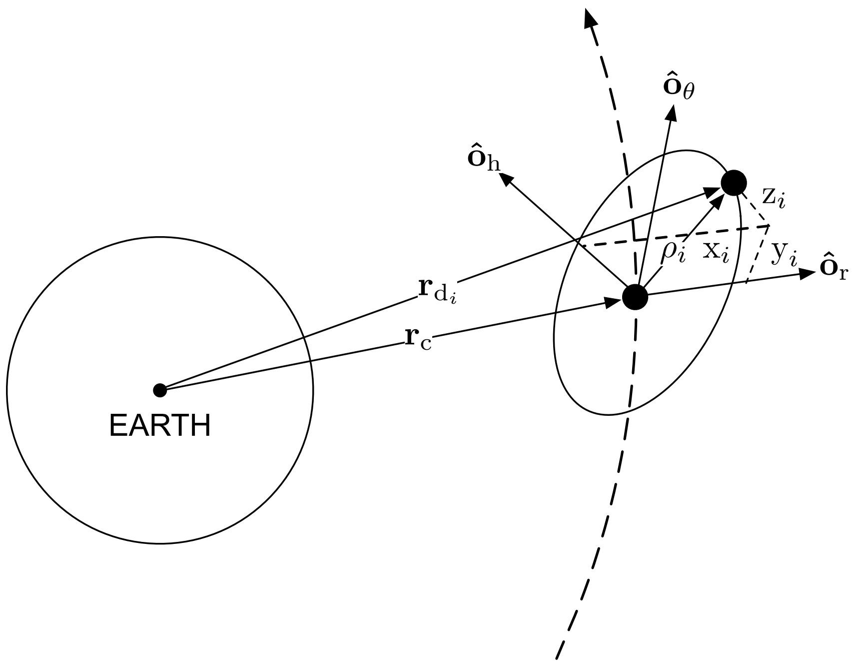

Figure 2.1: Illustration of Hill Frame Coordinate system

written as[7]

$$\ddot{x}_i - 2n\dot{y}_i - 3n^2 x_i = \sum_{j=1}^{N} \frac{k_c}{m_i} \frac{x_i - x_j}{d_{ij}^3} q_i q_j e^{-\frac{d_{ij}}{\lambda_d}} \tag{2.3a}$$

$$\ddot{y}_i + 2n\dot{x}_i = \sum_{j=1}^{N} \frac{k_c}{m_i} \frac{y_i - y_j}{d_{ij}^3} q_i q_j e^{-\frac{d_{ij}}{\lambda_d}} \tag{2.3b}$$

$$\ddot{z}_i + n^2 z_i = \sum_{j=1}^{N} \frac{k_c}{m_i} \frac{z_i - z_j}{d_{ij}^3} q_i q_j e^{-\frac{d_{ij}}{\lambda_d}} \tag{2.3c}$$

Here subscript i indicates the i^{th} position in the spacecraft formation, and d_{ij} is the distance between i^{th} and j^{th} spacecraft

$$d_{ij} = \sqrt{(x_i - x_j)^2 + (y_i - y_j)^2 + (z_i - z_j)^2} \tag{2.4}$$

To find a charged relative equilibrium, the relative acceleration and velocity of the spacecraft are set to zero, freezing the formation in the Hill frame. The individual spacecraft charges q_i can be scaled and written as

$$\tilde{q}_i = \frac{\sqrt{k_c}}{n} q_i \tag{2.5}$$

The normalized spacecraft charge $\tilde{q}_i$, is not a non-dimensional charge. Using equation (2.5) and the definition of charged product as $\tilde{Q}_{ij} = \tilde{q}_i \tilde{q}_j$, the equilibrium conditions are written as[7]

$$-3x_i = \sum_{i=1}^{N} \frac{1}{m_i} \frac{x_i - x_j}{d_{ij}^3} \tilde{Q}_{ij} \tag{2.6a}$$

$$0 = \sum_{i=1}^{N} \frac{1}{m_i} \frac{y_i - y_j}{d_{ij}^3} \tilde{Q}_{ij} \tag{2.6b}$$

$$z_i = \sum_{i=1}^{N} \frac{1}{m_i} \frac{z_i - z_j}{d_{ij}^3} \tilde{Q}_{ij} \tag{2.6c}$$

For a formation in which spacecraft are aligned in an along-track ($\hat{\mathbf{o}}_\theta$) direction, there are no charges required on the spacecraft to maintain the relative equilibrium. Such a formation is the naturally occurring equilibrium solution, and no charging effect is needed. Equations (2.6a)-(2.6c) are strongly coupled non-linear algebraic equations. The solutions to these equations are not intuitively obvious, thus the need for a numerical strategy. If the center the mass of the static formation is not aligned with Hill frame origin, the static formation will drift in the relative Hill frame space. Aligning the principal axes of the static formation with the Hill frame axes ensures that the gravity gradient torques are zero. Applying the center of mass and principal axes constraints reduces the search space for the solutions to exist. For a static formation to be an equilibrium solution, the center of mass and principal axes constraints must be satisfied.[15]

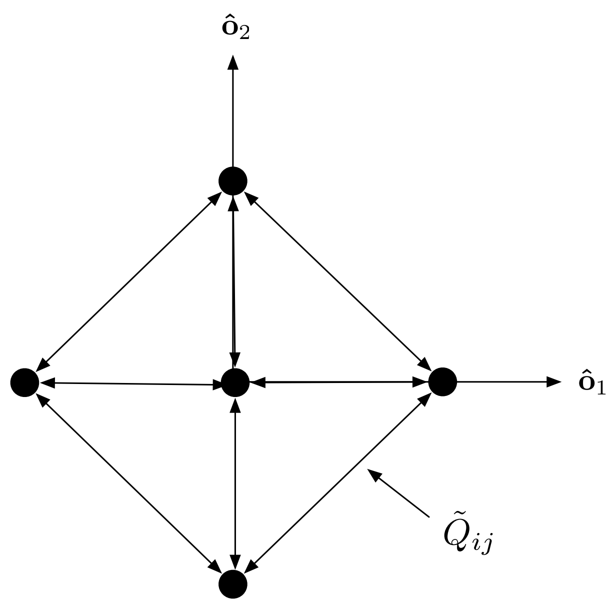

Figure 2.2: Planar 5-craft formation with CM and PA constraints satisfied

The center of mass and principal axes constraints are only necessary and not sufficient conditions for a static formation to exist. Figure 2.2 illustrates a 5-craft planar formation, where the center of mass and principal axes constraints are satisfied. The individual charges are computed from the charged product solutions found from equation(2.6a)-(2.6c). The charge products resulting from the equations (2.6a)-(2.6c) are not guaranteed to result in real or unique individual spacecraft charges. The individual charges on the spacecraft also have to satisfy these constraints imposed on the charged products. Thus the static Coulomb formation also needs to satisfy the constraints for the charged products. This makes the equations in (2.6a)-(2.6c) challenging and complex to solve.

Chapter 3

Analytic four-craft Static Coulomb Formation Solutions

To better understand the dynamics of a static Coulomb formation this chapter presents the analytic solutions for four-craft formations. Berryman and Schaub in Reference 7 present the analytic open-loop constant charge solutions for 2 and 3-craft formations. This chapter presents the analysis for a planar and three-dimensional four-craft formation. Charged product solutions are developed for each of the formation geometries, and a method to determine the individual spacecraft charges is presented. This chapter also presents the preliminary analysis for a co-linear four-craft formation. However the solution is not determined for a co-linear formations in this thesis. The necessary steps are developed to analyze the three-dimensional null-space of the co-linear formation. The work presented for the 1-D analysis serves as an open question on how to determine the open loop charges on a Coulomb structure with null-space dimension higher than 1. For the purposes of the analysis presented in this chapter, it is assumed that the spacecraft in the formations have equal masses.

3.1 Planar Formations

A planar formation lies in the principal planes defined by $\hat{\mathbf{o}}_r$-$\hat{\mathbf{o}}_h$, $\hat{\mathbf{o}}_r$-$\hat{\mathbf{o}}_\theta$ or $\hat{\mathbf{o}}_h$-$\hat{\mathbf{o}}_\theta$ planes. The formation lies entirely in these planes and there is no out of plane component. A square formation is one of the possible four-craft planar formations. The square formations have a potential use in missions such as interferometry . The center of mass condition can be satisfied by placing the center of the square at the origin of the Hill frame. The square is rotated in the principal plane about the third axis. By aligning this third rotation axis with one of the Hill frame axes, the principal axes constraint is satisfied. This section presents the analysis on determining the spacecraft charges for a square formation in one of the principal planes. The section also explores the uniqueness issue arising in a four-craft planar

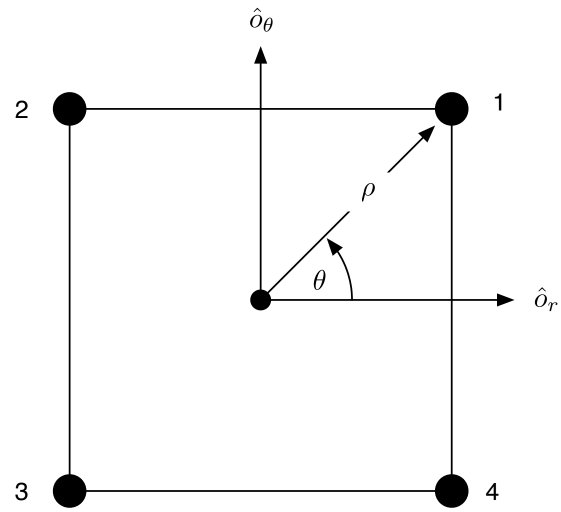

Figure 3.1: Planar 4-Satellite formation in $\hat{o}_r - \hat{o}_h$ plane

formatiom. The conditions for unique charges based on orientation of square in the principal plane are discussed.

3.1.1 Charge Products for Relative Equillibrium

A planar square formation can be parameterized in terms of the angle θ and the radius ρ as illustrated in figure 3.1. The angle θ represents the orientation of the square formation in any given plane. The radius ρ is the distance of the spacecraft from the origin of the Hill frame. Figure 3.1 shows the square formation in $\hat{\mathbf{o}}_r$-$\hat{\mathbf{o}}_\theta$ plane, where the square is rotated through an angle of $\theta = 45°$ from its nominal position of $\theta = 0°$. The square can be parametrized in a similar manner for $\hat{\mathbf{o}}_h$-$\hat{\mathbf{o}}_\theta$ and $\hat{\mathbf{o}}_r$-$\hat{\mathbf{o}}_h$ plane. For the formation in the $\hat{\mathbf{o}}_r$-$\hat{\mathbf{o}}_\theta$ plane, the position vectors of the 4 spacecraft are given by

$$\boldsymbol{\rho}_1 = \begin{pmatrix} \rho\cos\theta \\ \rho\sin\theta \\ 0 \end{pmatrix}, \quad \boldsymbol{\rho}_2 = \begin{pmatrix} -\rho\sin\theta \\ \rho\cos\theta \\ 0 \end{pmatrix}, \quad \boldsymbol{\rho}_3 = \begin{pmatrix} -\rho\cos\theta \\ -\rho\sin\theta \\ 0 \end{pmatrix}, \quad \boldsymbol{\rho}_4 = \begin{pmatrix} \rho\sin\theta \\ -\rho\cos\theta \\ 0 \end{pmatrix}$$

For a square formation there are 8 charged equations of motion from equation (2.6), 4 each in the $\hat{\mathbf{o}}_r$ and $\hat{\mathbf{o}}_\theta$ directions. The number of these equations is reduced by applying the center of mass conditions and principal axes constraints.[15] These conditions require that the center of mass of the static formation lie at the origin of the Hill frame, and the principal axes of the static formation be aligned with the axes of the rotating Hill frame. Due to symmetry for a planar formation there are 2 center of mass constraints and 1 principal axes constraint. The number of equations is now reduced to 5. Thus applying the center of mass and principal axes constraint and using equations (2.6a)−(2.6c), the formation dynamics in $\hat{o}_r - \hat{o}_\theta$ can be expressed in matrix form as

$$\begin{bmatrix} -3mx_1 \\ -3mx_2 \\ -3mx_3 \\ 0 \\ 0 \end{bmatrix} = \begin{bmatrix} \frac{x_1-x_2}{d_{12}^3} & \frac{x_1-x_3}{d_{13}^3} & \frac{x_1-x_4}{d_{14}^3} & 0 & 0 & 0 \\ \frac{x_2-x_1}{d_{12}^3} & 0 & 0 & \frac{x_2-x_3}{d_{23}^3} & \frac{x_2-x_4}{d_{24}^3} & 0 \\ 0 & \frac{x_3-x_1}{d_{13}^3} & 0 & \frac{x_3-x_2}{d_{23}^3} & 0 & \frac{x_3-x_4}{d_{34}^3} \\ \frac{y_1-y_2}{d_{12}^3} & \frac{y_1-y_3}{d_{13}^3} & \frac{y_1-y_4}{d_{14}^3} & 0 & 0 & 0 \\ \frac{y_2-y_1}{d_{12}^3} & 0 & 0 & \frac{y_2-y_3}{d_{23}^3} & \frac{y_2-y_4}{d_{24}^3} & 0 \end{bmatrix} \begin{bmatrix} \tilde{Q}_{12} \\ \tilde{Q}_{13} \\ \tilde{Q}_{14} \\ \tilde{Q}_{23} \\ \tilde{Q}_{24} \\ \tilde{Q}_{34} \end{bmatrix} \tag{3.1}$$

where $d_{ij} = \sqrt{(x_i - x_j)^2 + (y_i - y_j)^2}$ is the distance between the i^{th} and j^{th} spacecraft. Equation (3.1) can also be expressed in compact form as

$$\mathbf{x} = \mathbf{A}\tilde{\mathbf{Q}} \tag{3.2}$$

The matrix $\mathbf{A}$ only depends upon the orientation angle θ and the radius ρ of the spacecraft. It is interesting to note that the matrix $\mathbf{A}$ does not depend on the plane in which the formation is oriented. The null-space of $\mathbf{A}$ is constant for any given plane. To solve for the individual charges on spacecraft, a solution to the charged products $\tilde{Q}_{ij}$ is required. The matrix $\mathbf{A}$ in terms of angle θ and the radius ρ is written as

$$\mathbf{A} = \begin{bmatrix} \frac{\cos\theta+\sin\theta}{2\sqrt{2}\rho^2} & \frac{\cos\theta}{4\rho^2} & \frac{\cos\theta-\sin\theta}{2\sqrt{2}\rho^2} & 0 & 0 & 0 \\ \frac{-\cos\theta+\sin\theta}{2\sqrt{2}\rho^2} & 0 & 0 & \frac{\cos\theta-\sin\theta}{2\sqrt{2}\rho^2} & -\frac{\sin\theta}{4\rho^2} & 0 \\ 0 & -\frac{\cos\theta}{4\rho^2} & 0 & \frac{-\cos\theta+\sin\theta}{2\sqrt{2}\rho^2} & 0 & \frac{\cos\theta+\sin\theta}{2\sqrt{2}\rho^2} \\ \frac{-\cos\theta+\sin\theta}{2\sqrt{2}\rho^2} & \frac{\sin\theta}{4\rho^2} & \frac{\cos\theta+\sin\theta}{2\sqrt{2}\rho^2} & 0 & 0 & 0 \\ \frac{\cos\theta-\sin\theta}{2\sqrt{2}\rho^2} & 0 & 0 & \frac{\cos\theta+\sin\theta}{2\sqrt{2}\rho^2} & \frac{\cos\theta}{4\rho^2} & 0 \end{bmatrix} \tag{3.3}$$

The rank of matrix $\mathbf{A}$ is 5, and it is a full row rank matrix. There are infinitely many solutions to $\tilde{\mathbf{Q}}$, which can be expressed in terms of least squares solution, $\mathbf{Q}^*$, and the null-space $\mathbf{Q}_{\text{null}}$. The least squares solution for the system described by (3.2) is given by

$$\mathbf{Q}^* = \mathbf{A}^T \left(\mathbf{A}\mathbf{A}^T\right)^{-1} \mathbf{x} \tag{3.4}$$

All the possible solutions for $\tilde{\mathbf{Q}}$ are

$$\tilde{\mathbf{Q}} = \mathbf{Q}^* + t\mathbf{Q}_{\text{null}} \tag{3.5}$$

where t is a scalar used to scale the null space of $\mathbf{A}$. For the given $\hat{\mathbf{o}}_r$-$\hat{\mathbf{o}}_\theta$ plane, the least squares solution and the null space of the system are

$$\mathbf{Q}^* = \begin{bmatrix} -\frac{3\sqrt{2}}{10} m\rho^3 \left(4 + 5\sin 2\theta\right) \\ -\frac{6}{5} m\rho^3 \left(1 + 5\cos 2\theta\right) \\ \frac{3\sqrt{2}}{10} m\rho^3 \left(-4 + 5\sin 2\theta\right) \\ \frac{3\sqrt{2}}{10} m\rho^3 \left(-4 + 5\sin 2\theta\right) \\ -\frac{6}{5} m\rho^3 \left(1 - 5\cos 2\theta\right) \\ -\frac{3\sqrt{2}}{10} m\rho^3 \left(4 + 5\sin 2\theta\right) \end{bmatrix} \tag{3.6}$$

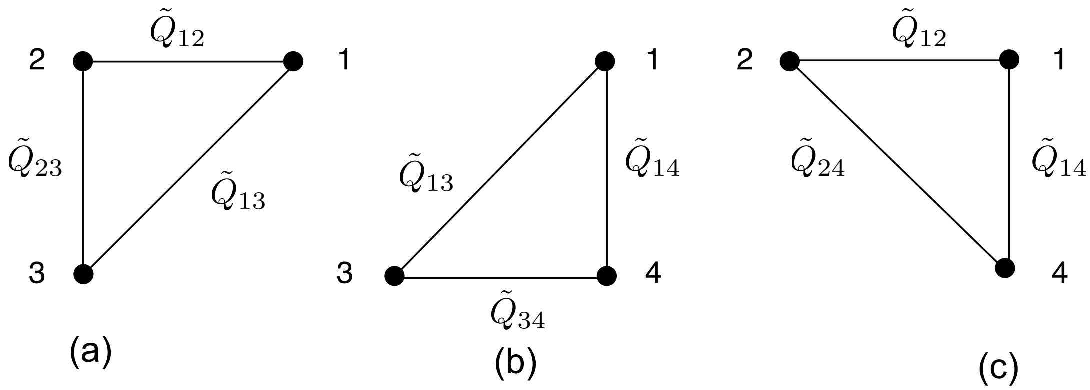

Figure 3.2: Breakdown of a square formation into triangular loops

$$\mathbf{Q}_{\text{null}} = \begin{bmatrix} 1 & -2\sqrt{2} & 1 & 1 & -2\sqrt{2} & 1 \end{bmatrix}^T \tag{3.7}$$

The least squares solution, for the $\hat{\mathbf{o}}_r$-$\hat{\mathbf{o}}_\theta$ plane depends on the size of the square formation and the orientation of the square in the plane. The null-space of the system does not depend on the orientation of the formation, and as discussed earlier is the same for any given plane.

3.1.2 Unique Spacecraft Charges

To implement a static Coulomb formation, knowledge of the individual charges on a spacecraft is required. For a four-craft formation, there are 6 charge products, which result in 4 individual spacecraft charges. This is always true for a four-craft formation, regardless of whether the formation is co-linear, planar or three-dimensional. There are infinitely many ways to solve for the individual charges from the charge products. To solve for $\tilde{q}_1$, we can break up the square into 3 different triangular loops about the spacecraft position 1 as shown in figure 3.2. From the loops defined in figure 3.2, $\tilde{q}_1$ can be calculated as

$$\tilde{q}_{1a} = \sqrt{\frac{\tilde{Q}_{12}\tilde{Q}_{13}}{\tilde{Q}_{23}}} \tag{3.8a}$$

$$\tilde{q}_{1b} = \sqrt{\frac{\tilde{Q}_{12}\tilde{Q}_{14}}{\tilde{Q}_{24}}} \tag{3.8b}$$

$$\tilde{q}_{1c} = \sqrt{\frac{\tilde{Q}_{14}\tilde{Q}_{13}}{\tilde{Q}_{34}}} \tag{3.8c}$$

For the individual charges on a spacecraft to be unique the equations (3.8a)-(3.8c) must yield the exact same value of $\tilde{q}_1$, which mathematically is written as

$$\tilde{q}_1 = \sqrt{\frac{\tilde{Q}_{12}\tilde{Q}_{13}}{\tilde{Q}_{23}}} = \sqrt{\frac{\tilde{Q}_{12}\tilde{Q}_{14}}{\tilde{Q}_{24}}} = \sqrt{\frac{\tilde{Q}_{14}\tilde{Q}_{13}}{\tilde{Q}_{34}}} \tag{3.9}$$

The charged products in the above equation depend on the scaling parameter t in the equation (3.5). Given a unique $\tilde{q}_1$, the remaining individual charges are trivially calculated as

$$\tilde{q}_2 = \frac{\tilde{Q}_{12}}{\tilde{q}_1} \tag{3.10a}$$

$$\tilde{q}_3 = \frac{\tilde{Q}_{13}}{\tilde{q}_1} \tag{3.10b}$$

$$\tilde{q}_4 = \frac{\tilde{Q}_{14}}{\tilde{q}_1} \tag{3.10c}$$

In a 3 spacecraft formation, there is only one triangular loop and it results in a unique individual charge. However, in a four-craft formation there are two additional triangular loops. These make the task of determining the individual spacecraft charges non-trivial. Assuming that $\tilde{q}_{1a}$ and $\tilde{q}_{1b}$ from equation (3.8a) and (3.8b) are equal.

$$\sqrt{\frac{\tilde{Q}_{12}\tilde{Q}_{13}}{\tilde{Q}_{23}}} = \sqrt{\frac{\tilde{Q}_{14}\tilde{Q}_{13}}{\tilde{Q}_{34}}} \tag{3.11}$$

Assuming $\tilde{Q}_{13} \neq 0$, equation (3.11) is simplified to

$$\tilde{Q}_{12}\tilde{Q}_{34} - \tilde{Q}_{14}\tilde{Q}_{23} = 0 \tag{3.12}$$

Using equations (3.5)-(3.7), equation (3.12) is written as

$$\left(-\frac{3\sqrt{2}}{10}m\rho^3\left(4 + 5\sin 2\theta\right) + t\right)^2 - \left(-\frac{3\sqrt{2}}{10}m\rho^3\left(4 - 5\sin 2\theta\right) + t\right)^2 = 0 \tag{3.13}$$

Simplifying further

$$\frac{6}{5}m\rho^3\left(-5\sqrt{2}t + 12m\rho^3\right)\sin\left(2\theta\right) = 0 \tag{3.14}$$

Thus the quadratic equation in (3.13) simplifies to a linear equation with one root, which can be solved for t where the individual charges are unique. Equation (3.14) is also true when $\sin 2\theta = 0$. Thus unique charges can be found for specific orientation angles of $\theta = 0°$ and $\theta = 90°$. Such an orientation corresponds to two spacecraft aligned along the $\hat{\mathbf{o}}_h$ axes and the remaining 2 spacecraft aligned along the $\hat{\mathbf{o}}_r$ axes. Solving equation (3.14), the value of t for which the equation (3.11) holds true is

$$t = \frac{6\sqrt{2}}{5} m\rho^3 \tag{3.15}$$

The value of scalar t in equation (3.15) ensures that a unique $\tilde{q}_1$ is found from two loops (a) and (b) in figure 3.2. To prove that the third equality constraint is satisfied, let us explore the third uniqueness condition in equation (3.8c). The equation (3.8c) can also be written as

$$\tilde{q}_{1c} = \sqrt{\frac{\tilde{Q}_{14}\tilde{Q}_{12}}{\tilde{Q}_{24}} \cdot \frac{\tilde{Q}_{13}\tilde{Q}_{24}}{\tilde{Q}_{34}\tilde{Q}_{12}}} = \sqrt{\tilde{q}_{1b}^2 \cdot \frac{\tilde{Q}_{13}\tilde{Q}_{24}}{\tilde{Q}_{34}\tilde{Q}_{12}}} \tag{3.16}$$

Thus it is seen that equation (3.8c) is same as (3.8b) if

$$\frac{\tilde{Q}_{13}\tilde{Q}_{24}}{\tilde{Q}_{34}\tilde{Q}_{12}} = 1 \tag{3.17}$$

Using the value of scaling parameter t from (3.15) and equations (3.6) and (3.7), the equation (3.5) is rewritten as

$$\tilde{\mathbf{Q}} = m\rho^3 \begin{bmatrix} -3\sqrt{2}\cos\theta\sin\theta \\ -3\sqrt{2}\cos^2\theta \\ 3\sqrt{2}\cos\theta\sin\theta \\ 3\sqrt{2}\cos\theta\sin\theta \\ -3\sqrt{2}\sin^2\theta \\ -3\sqrt{2}\cos\theta\sin\theta \end{bmatrix} \tag{3.18}$$

Using the values of $\tilde{Q}_{ij}$ from equation (3.18), equation (3.17) is rewritten as

$$\frac{\tilde{Q}_{13}\tilde{Q}_{24}}{\tilde{Q}_{34}\tilde{Q}_{12}} = \frac{\left(-3\sqrt{2}\sin^2\theta\right)\left(-3\sqrt{2}\cos^2\theta\right)}{\left(-3\sqrt{2}\sin\theta\cos\theta\right)\left(-3\sqrt{2}\sin\theta\cos\theta\right)} = 1 \tag{3.19}$$

Thus the condition in equation (3.8c) is satisfied and that the equation (3.8c) will yield the same $\tilde{q}_1$ as (3.8b). It is shown that to obtain a unique spacecraft charge only one equality constraints from equations (3.8a)- (3.8c) needs to be satisfied, as the second one is guaranteed to be true. This argument is only true for a square planar formation with equal spacecraft masses.

Carefully choosing the value of the null-space scaling parameter t, the number of equality constraints for unique spacecraft charges are reduced to 1. This method does not take into consideration that unique spacecraft charges exist for specific orientation angles of $\theta = 0°$ and $\theta = 90°$. For $\theta = 0°$, the charged products solutions is

$$\tilde{\mathbf{Q}} = \begin{bmatrix} t - \frac{6}{5}\sqrt{2}m\rho^3 \\ -2\sqrt{2}t - \frac{36}{5}m\rho^3 \\ t - \frac{6}{5}\sqrt{2}m\rho^3 \\ t - \frac{6}{5}\sqrt{2}m\rho^3 \\ -2\sqrt{2}t + \frac{24}{5}m\rho^3 \\ t - \frac{6}{5}\sqrt{2}m\rho^3 \end{bmatrix} \tag{3.20}$$

It is seen from equation (3.20,) that only 1 equality constraint needs to be satisfied for unique spacecraft charges as $\tilde{Q}_{12}\tilde{Q}_{34} = \tilde{Q}_{14}\tilde{Q}_{23}$. The null-space scaling parameter t can be chosen in a manner such that equation (3.17) is satisfied. Using the values of charged production from (3.20), equation (3.17) is rewritten as

$$7t^2 - \frac{36}{5}\sqrt{2}m\rho^3 t + \frac{936}{5}m^2\rho^6 = 0 \tag{3.21}$$

Equation (3.21) is a quadratic equation. There are two possible values of null-space scaling parameter t where unique charges can be found for orientation angle $\theta = 0°$. Solving equation (3.21) the values of t for which unique spacecraft charges exist are

$$t_1 = \frac{6}{5}\sqrt{2}m\rho^3 \tag{3.22a}$$
$$t_2 = -\frac{78}{35}\sqrt{2}m\rho^3 \tag{3.22b}$$

From equation (3.22a) it is noted that the value of null-space scaling parameter t is same as in equation (3.15). This implies that it is possible for find real spacecraft charges for orientations other than $\theta = 0°$ or $\theta = 90°$. However if the null-space scaling parameter is used from equation (3.22b), then real charges can only be found for $\theta = 0°$ or $\theta = 90°$. The steps in equations (3.20) to (3.22) for $\theta = 90°$. For $\theta = 90°$, the null-space scaling parameter for unique charges is the same as in equation (3.22).

Without loss of generality, the steps from equations (3.8) to (3.22) can be repeated for the other two planes $\hat{\mathbf{o}}_h$-$\hat{\mathbf{o}}_\theta$ and $\hat{\mathbf{o}}_r$-$\hat{\mathbf{o}}_h$. The formation dynamics in $\hat{\mathbf{o}}_h$-$\hat{\mathbf{o}}_\theta$ can be written as

$$m\begin{bmatrix} -3z_1 \\ -3z_2 \\ -3z_3 \\ 0 \\ 0 \end{bmatrix} = \begin{bmatrix} \frac{\cos\theta+\sin\theta}{2\sqrt{2}\rho^2} & \frac{\cos\theta}{4\rho^2} & \frac{\cos\theta-\sin\theta}{2\sqrt{2}\rho^2} & 0 & 0 & 0 \\ \frac{-\cos\theta+\sin\theta}{2\sqrt{2}\rho^2} & 0 & 0 & \frac{\cos\theta-\sin\theta}{2\sqrt{2}\rho^2} & -\frac{\sin\theta}{4\rho^2} & 0 \\ 0 & -\frac{\cos\theta}{4\rho^2} & 0 & \frac{-\cos\theta+\sin\theta}{2\sqrt{2}\rho^2} & 0 & \frac{\cos\theta+\sin\theta}{2\sqrt{2}\rho^2} \\ \frac{-\cos\theta+\sin\theta}{2\sqrt{2}\rho^2} & \frac{\sin\theta}{4\rho^2} & \frac{\cos\theta+\sin\theta}{2\sqrt{2}\rho^2} & 0 & 0 & 0 \\ \frac{\cos\theta-\sin\theta}{2\sqrt{2}\rho^2} & 0 & 0 & \frac{\cos\theta+\sin\theta}{2\sqrt{2}\rho^2} & \frac{\cos\theta}{4\rho^2} & 0 \end{bmatrix} \begin{bmatrix} \tilde{Q}_{12} \\ \tilde{Q}_{13} \\ \tilde{Q}_{14} \\ \tilde{Q}_{23} \\ \tilde{Q}_{24} \\ \tilde{Q}_{34} \end{bmatrix} \tag{3.23}$$

Equation (3.12) for $\hat{\mathbf{o}}_h$-$\hat{\mathbf{o}}_\theta$ plane is written as

$$-\frac{2}{5}m\rho^3\left(5\sqrt{2}t+4m\rho^3\right)\sin 2\theta = 0 \tag{3.24}$$

The value of t for which the unique spacecraft charges can be found is.

$$t = \frac{-4}{5\sqrt{2}}m\rho^3 \tag{3.25}$$

Unique spacecraft charges can also be computed for $\theta = 0\circ$ or $\theta = 90°$. The null-space scaling factor t required for unique spacecraft charges is

$$t_1 = -\frac{4}{5\sqrt{2}}m\rho^3 \tag{3.26a}$$
$$t_2 = \frac{52}{35\sqrt{2}}m\rho^3 \tag{3.26b}$$

It is noted that the value of null-space scaling factor in (3.26a) is the same as in equation (3.25). Thus real charges can be computed for any orientation of square in the $\hat{\mathbf{o}}_h$-$\hat{\mathbf{o}}_\theta$ plane. However if the value of scaling parameter from equation (3.26a) is used, real charges can only be computed for $\theta = 0°$ or $\theta = 90°$.

The formation dynamics in the $\hat{\mathbf{o}}_r$-$\hat{\mathbf{o}}_h$ plane is written as

$$m\begin{bmatrix} -3x_1 \\ -3x_2 \\ -3x_3 \\ z_1 \\ z_2 \end{bmatrix} = \begin{bmatrix} \frac{\cos\theta+\sin\theta}{2\sqrt{2}\rho^2} & \frac{\cos\theta}{4\rho^2} & \frac{\cos\theta-\sin\theta}{2\sqrt{2}\rho^2} & 0 & 0 & 0 \\ \frac{-\cos\theta+\sin\theta}{2\sqrt{2}\rho^2} & 0 & 0 & \frac{\cos\theta-\sin\theta}{2\sqrt{2}\rho^2} & -\frac{\sin\theta}{4\rho^2} & 0 \\ 0 & -\frac{\cos\theta}{4\rho^2} & 0 & \frac{-\cos\theta+\sin\theta}{2\sqrt{2}\rho^2} & 0 & \frac{\cos\theta+\sin\theta}{2\sqrt{2}\rho^2} \\ \frac{-\cos\theta+\sin\theta}{2\sqrt{2}\rho^2} & \frac{\sin\theta}{4\rho^2} & \frac{\cos\theta+\sin\theta}{2\sqrt{2}\rho^2} & 0 & 0 & 0 \\ \frac{\cos\theta-\sin\theta}{2\sqrt{2}\rho^2} & 0 & 0 & \frac{\cos\theta+\sin\theta}{2\sqrt{2}\rho^2} & \frac{\cos\theta}{4\rho^2} & 0 \end{bmatrix} \begin{bmatrix} \tilde{Q}_{12} \\ \tilde{Q}_{13} \\ \tilde{Q}_{14} \\ \tilde{Q}_{23} \\ \tilde{Q}_{24} \\ \tilde{Q}_{34} \end{bmatrix} \tag{3.27}$$

Equation (3.12) for $\hat{\mathbf{o}}_h$-$\hat{\mathbf{o}}_\theta$ plane is written as

$$-\frac{2}{5}m\rho^3\left(5\sqrt{2}t+4m\rho^3\right)\sin 2\theta = 0 \tag{3.28}$$

The value of t for which the unique spacecraft charges can be found is.

$$t = \frac{4}{5}\sqrt{2}m\rho^3 \tag{3.29}$$

Unique spacecraft charges can also be computed for $\theta = 0°$ or $\theta = 90°$. The null-space scaling factor t required for unique spacecraft charges is

$$t_1 = -\frac{4}{35}m\rho^3\left(3\sqrt{2}-5\sqrt{29}\right) \tag{3.30a}$$
$$t_2 = -\frac{4}{35}m\rho^3\left(3\sqrt{2}+5\sqrt{29}\right) \tag{3.30b}$$

It is noted that unlike $\hat{\mathbf{o}}_r$-$\hat{\mathbf{o}}_\theta$ and $\hat{\mathbf{o}}_h$-$\hat{\mathbf{o}}_\theta$ planes the value of null-space scaling factor in (3.30) is not common to the scaling parameter for arbitrary orientations. Real charges can be computed for any orientation of square in the $\hat{\mathbf{o}}_r$-$\hat{\mathbf{o}}_h$ plane using the scaling parameter in equation (3.29). If the value of scaling parameter from equation (3.30b) or (3.30a) is used, real charges can only be computed for $\theta = 0\circ$ or $\theta = 90°$.

From equations (3.15),(3.25) and (3.29), it is evident that for an arbitrary orientation of a formation in the given plane, only one set of unique individual charges on the spacecraft exists. Further the value of the scalar t where these unique charges exist is a constant in a given plane and does not depend on the orientation θ of the formation within the given plane. However it is also possible to find unique spacecraft charges for specific orientations of $\theta = 0°$ or $\theta = 90°$.

3.1.3 Real Charges

Finding unique spacecraft charges is not a sufficient condition for the formation to exist; the charges on the spacecraft in a formation also need to be real. In a 3-craft formation, there is only one inequality constraint for real charges. For a four-craft formation, there are two additional constraints. Mathematically the conditions for real charges are expressed as the inequality constraints

$$\tilde{Q}_{12} \cdot \tilde{Q}_{13} \cdot \tilde{Q}_{23} > 0 \tag{3.31a}$$

$$\tilde{Q}_{12} \cdot \tilde{Q}_{14} \cdot \tilde{Q}_{24} > 0 \tag{3.31b}$$

$$\tilde{Q}_{13} \cdot \tilde{Q}_{14} \cdot \tilde{Q}_{34} > 0 \tag{3.31c}$$

For real spacecraft charges in a 3-craft formation the inequality constraint in equation (3.31a) needs to be true. The additional constraints for real spacecraft in equations (3.31b) and (3.31c) need to be satisfied for a four-craft formation. Using (3.8a) equation (3.31a) can be written as

$$\tilde{q}_1^2 \cdot \left(\tilde{Q}_{23}\right)^2 > 0 \tag{3.32}$$

Assuming the real charge condition in equation (3.31a) is satisfied. We find $\tilde{q}_1^2 > 0$ as $\tilde{Q}_{23}^2 > 0$ for all values of $\tilde{Q}_{23}$. Similarly equations (3.31b) and (3.31c) are expressed as

$$\tilde{q}_1^2 \cdot \left(\tilde{Q}_{24}\right)^2 > 0 \tag{3.33}$$

$$\tilde{q}_1^2 \cdot \left(\tilde{Q}_{34}\right)^2 > 0 \tag{3.34}$$

Because it was already proven that $q_1^2 > 0$ as equation (3.31a) is true; the other two inequality constraints (3.31b) and (3.31c) are guaranteed to be satisfied. While the individual charge $\tilde{q}_1$ is the unique spacecraft charge required on a formation. The arguments in equations (3.31a)-(3.31c) are valid for any four-craft formation, not just the special case of square formation being considered here.

Using the null-space of $\tilde{\mathbf{Q}}$ in (3.5) equation (3.31a) is expanded as a cubic polynomial in terms of the scalar t. The roots of this polynomial expressed in terms of θ and ρ are

$$\begin{aligned} t_1 &= -\tfrac{3}{5\sqrt{2}} m\rho^3 \left(1 + 5\cos 2\theta\right) \\ t_2 &= \tfrac{3}{5\sqrt{2}} m\rho^3 \left(2 - 5\sin 2\theta\right) \\ t_3 &= \tfrac{3}{5\sqrt{2}} m\rho^3 \left(2 + 5\sin 2\theta\right) \end{aligned} \tag{3.35}$$

The range of t for which the inequality constraint (3.31a) is satisfied, can be determined in terms of the roots in equation (3.35). Wang in reference 27 exploits the 1-D null-space to parametrize the inequality constraint for real charges. For the 1-D constrained 3-craft he presents an elegant method for determining the regions of real charges in terms of the roots in equation (3.31a). Let $\hat{a}$, $\hat{b}$ and $\hat{c}$ represent Q_{12}^*, Q_{13}^* and Q_{23}^* respectively from (3.6), using this parametrization and (3.7), equation(3.31a) can be written down as

$$f\left(t\right) = \left(\hat{a} + t\right)\left(\hat{b} - 2\sqrt{2}t\right)\left(\hat{c} + t\right) > 0 \tag{3.36}$$

Let a, b and c be the roots of the polynomial in (3.36), arranged in the following order $a > b > c$. An interesting property of the polynomial in (3.36) is as $\lim_{t\to\infty} f\left(t\right) < 0$ and $\lim_{t\to-\infty} f\left(t\right) > 0$. Thus the inequality constraint in (3.31a) is satisfied in the region b $< t <$ a and $t <$ c.

Figure 3.3(a) shows the shape of the general polynomial described by equation (3.36) and the valid regions of t where $f\left(t\right) > 0$. Figure 3.3(b) plots $\tilde{t}_i$ for $0° \leq \theta \leq 90°$, where $\tilde{t}_i = \frac{5\sqrt{2}}{3m\rho^3} t_i$. The shaded regions show the range of θ where the individual charges are real. Figure 3.3(b) also plots the value of null-space scaling factor for unique charges in equation (3.22). For a solution to exist, the value of t in (3.22) and should lie in the shaded region of the plot in figure 3.3(b). From the figure we can see for the individual charges to be real and implementable, the square can be rotated between $0 \leq \theta \leq 90$ degrees from $\hat{\mathbf{o}}_r$ axis for the formation to be possible. Table 1 shows the order of roots arranged in terms of the orientation of the square in the $\hat{\mathbf{o}}_r$-$\hat{\mathbf{o}}_\theta$ plane.

θ	Order of Roots
$0 < \theta < 45$	$t_2 > t_3 > t_1$
$45 < \theta < 90$	$t_2 > t_1 > t_3$

Table 3.1: Order of Roots depending on angle of orientation for $\hat{o}_r - \hat{o}_\theta$ plane

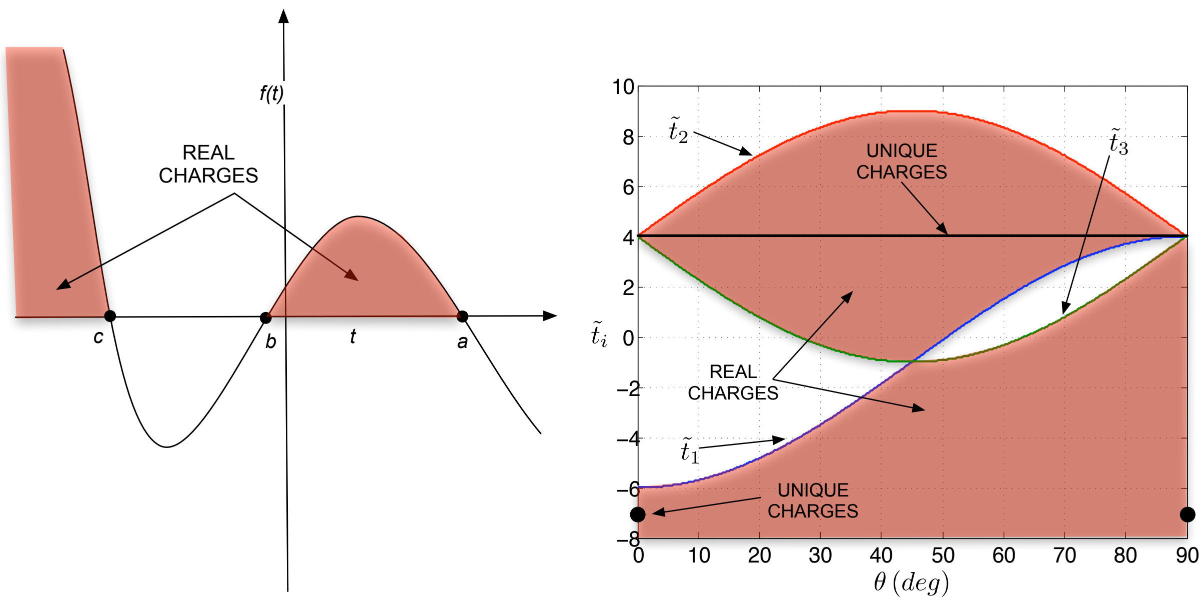

(a) Valid regions for charges to be real for $\theta = 30°$

(b) Range of θ for real charges for $\hat{o}_r - \hat{o}_\theta$ plane

Figure 3.3: Plot of regions where unique spacecraft charges are real

The individual charges now can be calculated by substituting in the value of t from (3.15) in equation (3.8a) to get q_1 in terms of ρ and θ.

$$\tilde{q}_1 = \sqrt{3\sqrt{2}m\rho^3}\cos\theta \tag{3.37a}$$

$$\tilde{q}_2 = \sqrt{3\sqrt{2}m\rho^3}\sin\theta \tag{3.37b}$$

$$\tilde{q}_3 = -\sqrt{3\sqrt{2}m\rho^3}\cos\theta \tag{3.37c}$$

$$\tilde{q}_4 = -\sqrt{3\sqrt{2}m\rho^3}\sin\theta \tag{3.37d}$$

The individual charges found in equation (3.37) are only valid for $t = \frac{6}{5}\sqrt{2}m\rho^3$. From figure 3.3(b) it can be seen that for $\theta = 0°$ or $\theta = 90°$ and $t = \frac{6}{5}\sqrt{2}m\rho^3$ unique and real spacecraft charges exist. While $\theta = 0°$ spacecraft 2 and 4 are aligned along $\hat{\mathbf{o}}_\theta$ axis and have no charges acting on them. It is also noted when $t = \frac{6}{5}\sqrt{2}m\rho^3$ unique and real charges exist for formation orientations other than $\theta = 0°$ or $\theta = 90°$. It is also observed that when $t = -\frac{78}{35}\sqrt{2}m\rho^3$ real spacecraft charges only exist for $\theta = 0°$ or $\theta = 90°$. This is true because $\theta = 0°$ or $\theta = 90°$

are the only possible orientations for the unique charges. However in this case the charges on spacecraft aligned along the $\hat{\mathbf{o}}_\theta$ axis is not 0. The individual charges for such a formation are given by

$$\tilde{q}_1 = 2\sqrt{\frac{3}{7}}\sqrt{m\rho^3} \tag{3.38a}$$

$$\tilde{q}_2 = -4\sqrt{\frac{6}{7}}\sqrt{m\rho^3} \tag{3.38b}$$

$$\tilde{q}_3 = -2\sqrt{\frac{3}{7}}\sqrt{m\rho^3} \tag{3.38c}$$

$$\tilde{q}_4 = 4\sqrt{\frac{6}{7}}\sqrt{m\rho^3} \tag{3.38d}$$

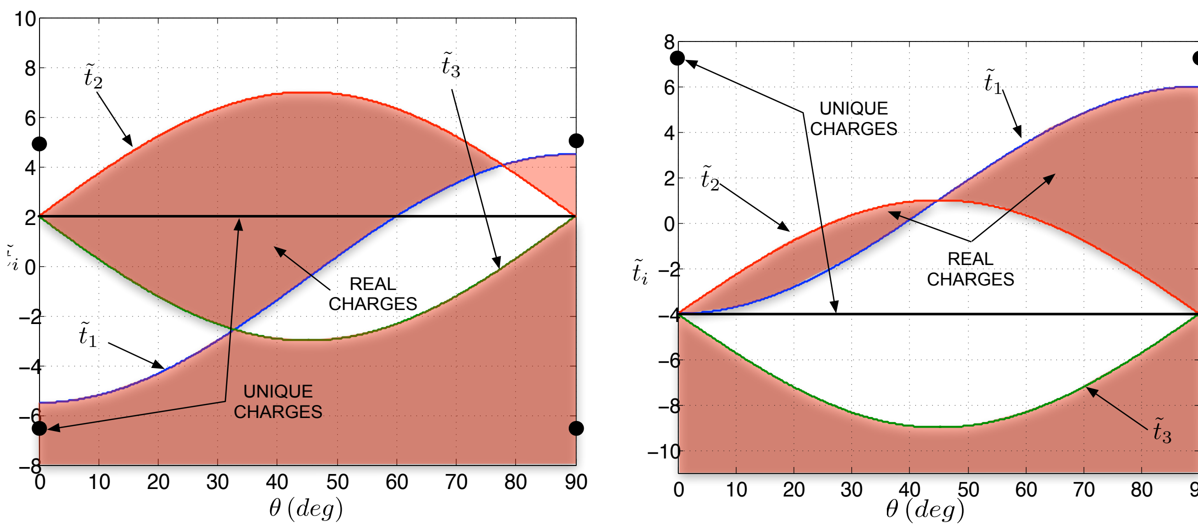

(a) $\hat{\mathbf{o}}_{\mathbf{r}}$-$\hat{\mathbf{o}}_h$ (b) $\hat{\mathbf{o}}_{\mathbf{h}}$-$\hat{\mathbf{o}}_\theta$

Figure 3.4: Plot of θ for real and unique charges.

As discussed earlier, the regions where charges are real and unique charges for $\hat{\mathbf{o}}_h$-$\hat{\mathbf{o}}_\theta$ and $\hat{\mathbf{o}}_r$-$\hat{\mathbf{o}}_h$ plane and consequently the individual charges themselves can be determined easily using the analysis presented for $\hat{\mathbf{o}}_r$-$\hat{\mathbf{o}}_\theta$ plane. Figures 3.4(a) and 3.4(b) show the plots of $\tilde{t}_i$ vs. θ for $\hat{\mathbf{o}}_r$-$\hat{\mathbf{o}}_h$ and $\hat{\mathbf{o}}_h$-$\hat{\mathbf{o}}_\theta$ plane respectively. Here the shaded area indicates the region for real spacecraft charges. The individual charges for $\hat{\mathbf{o}}_r$-$\hat{\mathbf{o}}_h$ plane can be calculated by plugging in the value of t from (3.29) in equation (3.8a) to get $\tilde{q}_1$ in terms of ρ and θ, where $0 \le \theta \le 60$

$$\tilde{q}_1 = 2\sqrt{m\rho^3\,(1 + 2\cos 2\theta)} \tag{3.39a}$$

$$\tilde{q}_2 = \sqrt{2m\rho^3\left(1 + 2\cos 2\theta\right)} \tag{3.39b}$$

$$\tilde{q}_3 = -2\sqrt{m\rho^3\left(1 + 2\cos 2\theta\right)} \tag{3.39c}$$

$$\tilde{q}_4 = -\sqrt{2m\rho^3\left(1 + 2\cos 2\theta\right)} \tag{3.39d}$$

It is noted that for $\hat{\mathbf{o}}_h$-$\hat{\mathbf{o}}_\theta$ plane that the value of null-space scaling factor in equation (3.30a) does not yield real spacecraft charges for specific orientations of $\theta = 0°$ and $\theta = 90°$. The scaling factor from equation (3.30b) however allows the computation of real and spacecraft charge. The individual spacecraft charges are computed as

$$\tilde{q}_1 = \frac{1267}{1122}\sqrt{m\rho^3} \tag{3.40a}$$

$$\tilde{q}_2 = \frac{1409}{678}\sqrt{m\rho^3} \tag{3.40b}$$

$$\tilde{q}_3 = -\frac{1267}{1122}\sqrt{m\rho^3} \tag{3.40c}$$

$$\tilde{q}_4 = -\frac{1409}{678}\sqrt{m\rho^3} \tag{3.40d}$$

From figure 3.4(b) it is evident that a square formation in $\hat{\mathbf{o}}_h$-$\hat{\mathbf{o}}_\theta$ plane only exists for $\theta = 0$ deg or $\theta = 90$ deg. Figure 3.5 illustrates the only possible orientation of the square in $\hat{\mathbf{o}}_\mathbf{h}$-$\hat{\mathbf{o}}_\theta$ plane. The individual charges on spacecraft 2 and 4 are zero, as they lie along the $\hat{\mathbf{o}}_\theta$ plane. The square formation thus simplifies to a linear 2-craft formation in $\hat{\mathbf{o}}_h$ plane, solution to which has been discussed by Berryman and Schaub in reference 7. It is also noted from figure 3.4(b) that the value of null-space scaling factor in equation (3.26b) does not yield real spacecraft charges.

3.2 Three-Dimensional Formations

A tetrahedron is the one of the possible three-dimensional formations which satisfies the center of mass and the principal axes constraint for virtual Coulomb structures. An elegant property of tetrahedron is that the principal axes of tetrahedron can be aligned arbitrarily, and are aligned in such a manner that the principal axes constraint is satisfied. Figure 3.6 shows the top and front view of a tetrahedron aligned along the $\hat{\mathbf{o}}_r$ axes. Spacecraft 1 is placed along the $\hat{\mathbf{o}}_r$ axes, the vertex of the tetrahedron. The remaining spacecraft form

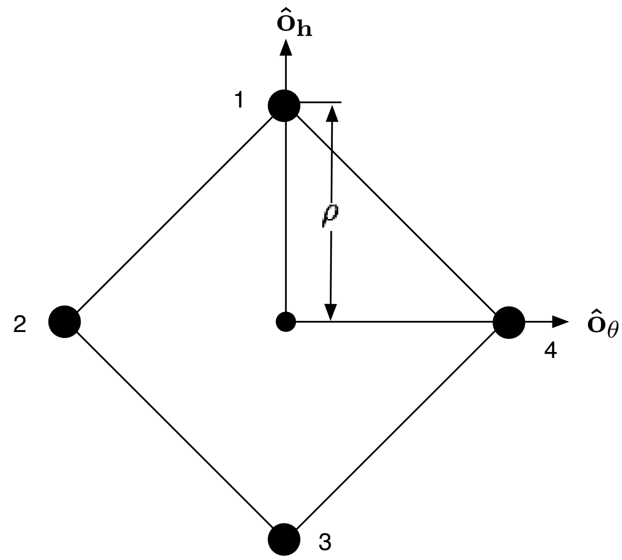

Figure 3.5: Orientation of a square in $\hat{o}_h - \hat{o}_\theta$ plane

an equilateral triangle in the $\hat{\mathbf{o}}_h$-$\hat{\mathbf{o}}_\theta$ plane. The body frame coordinates of the tetrahedron aligned along $\hat{\mathbf{o}}_r$ axes is given by

$$\boldsymbol{\rho}_1 = \begin{pmatrix} \rho \\ 0 \\ 0 \end{pmatrix}, \ \boldsymbol{\rho}_2 = \begin{pmatrix} -\frac{\rho}{3} \\ 0 \\ \frac{-2\sqrt{2}\rho}{3} \end{pmatrix}, \ \boldsymbol{\rho}_3 = \begin{pmatrix} -\frac{\rho}{3} \\ \frac{\sqrt{2}\rho}{\sqrt{3}} \\ \frac{\sqrt{2}\rho}{3} \end{pmatrix}, \ \boldsymbol{\rho}_4 = \begin{pmatrix} -\frac{\rho}{3} \\ \frac{-\sqrt{2}\rho}{\sqrt{3}} \\ \frac{\sqrt{2}\rho}{3} \end{pmatrix}$$

Here the body frame of the tetrahedron is aligned with the Hill frame. There are several different attitude descriptions available to represent the orientation of the body frame with respect to the Hill frame. A sequence of Euler angles is used in the analysis presented here to describe the orientation of the body frame.

3.2.1 Three-Dimensional Rotation of Tetrahedron

Let ψ, θ and ϕ represent the rotation angles about $\hat{\mathbf{o}}_\mathbf{r}$, $\hat{\mathbf{o}}_\theta$ and $\hat{\mathbf{o}}_\mathbf{h}$ axis respectively. The rotation matrix for a sequential 1-3-2 Euler angle rotation is given by[24]

$$C = \begin{bmatrix} \cos\theta\cos\phi & \cos\theta\cos\psi\sin\phi + \sin\theta\sin\psi & -\cos\psi\sin\theta + \cos\theta\sin\phi\sin\psi \\ -\sin\phi & \cos\phi\cos\psi & \cos\theta\sin\psi \\ \cos\phi\sin\theta & \cos\psi\sin\theta\sin\phi - \cos\sin\psi & \cos\theta\cos\psi + \sin\theta\sin\phi\sin\psi \end{bmatrix} \tag{3.41}$$

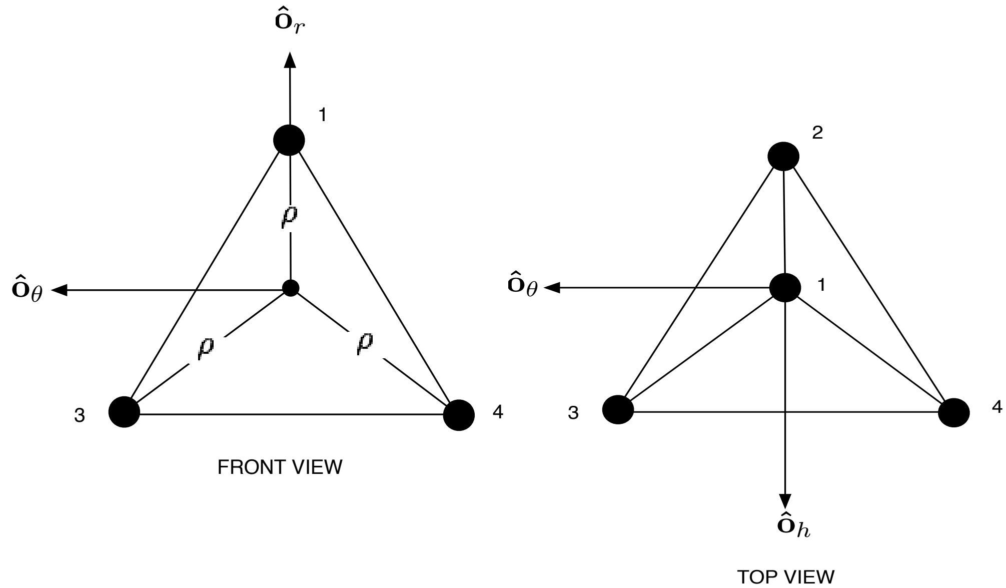

Figure 3.6: Parametrization of a Tetrahedron

Using the rotation matrix, the Hill frame position coordinates can now be expressed as

$$\rho_1 = \rho \begin{pmatrix} c\theta\ c\phi \\ s\phi\ c\theta\ c\psi + s\theta\ s\psi \\ -c\psi\ s\theta + c\theta\ s\phi\ s\psi \end{pmatrix} \tag{3.42a}$$

$$\rho_2 = \frac{1}{3}\rho \begin{pmatrix} -c\phi\left(c\theta + 2\sqrt{2}s\theta\right) \\ -s\theta\left(2\sqrt{2}c\psi\ s\phi + s\psi\right) - c\theta\left(c\psi\ s\phi - 2\sqrt{2}s\psi\right) \\ c\psi\ s\theta - c\theta\ s\phi\ s\psi - 2\sqrt{2}\left(c\theta\ c\psi + s\theta\ s\phi\ s\psi\right)\end{pmatrix} \tag{3.42b}$$

$$\rho_3 = \frac{1}{3}\rho \begin{pmatrix} -c\phi\left(c\theta - \sqrt{2}s\theta\right) - \sqrt{6}s\phi \\ \sqrt{6}c\phi\ c\psi - c\psi\ s\phi\left(c\theta - \sqrt{2}s\theta\right) - s\psi\left(\sqrt{2}c\theta + s\theta\right) \\ \sqrt{6}c\phi\ s\psi + c\theta\left(\sqrt{2}c\psi - s\phi\ s\psi\right) + s\theta\left(c\phi + \sqrt{2}s\phi\ s\psi\right)\end{pmatrix} \tag{3.42c}$$

$$\rho_4 = \frac{1}{3}\rho \begin{pmatrix} -c\theta\ c\phi + \sqrt{2}c\phi\ s\theta + \sqrt{6}s\phi \\ -\sqrt{6}c\phi\ c\psi - c\psi\ s\phi\left(c\theta - \sqrt{2}s\theta\right) - s\psi\left(\sqrt{2}c\theta + s\theta\right) \\ -\sqrt{6}c\phi\ s\psi + c\theta\left(\sqrt{2}c\psi - s\phi\ s\psi\right) + s\theta\left(c\phi + \sqrt{2}s\phi\ s\psi\right)\end{pmatrix} \tag{3.42d}$$

Here the short hand notation $c = \cos\alpha$ and $s = \sin\alpha$ is used. It is seen from the equation (3.42), that analysis of a full three-dimensional rotation tetrahedron is complex for arbitrary orientations. Analysis of a 2 angle rotation of tetrahedron for a range of the third angle provides a family of solutions for which a virtual tetrahedron exists. For the analysis presented here the rotation about the $\hat{\mathbf{o}}_{\mathbf{r}}$ axis, ψ is set to 0°. The Hill frame position coordinates after a $\hat{\mathbf{o}}_{\mathbf{h}}$-$\hat{\mathbf{o}}_{\theta}$ sequence can be written down using the rotation matrix in equation (3.41)

$$\rho_1 = \rho \begin{pmatrix} \cos\theta\cos\phi \\ \sin\phi\cos\theta \\ \sin\theta \end{pmatrix} \tag{3.43a}$$

$$\rho_2 = \frac{1}{3}\rho \begin{pmatrix} -cos\phi\left(\cos\theta + 2\sqrt{2}\sin\theta\right) \\ \sin\phi\left(-2\sqrt{2}\sin\theta - \cos\theta\right) \\ \sin\theta - 2\sqrt{2}\cos\theta \end{pmatrix} \tag{3.43b}$$

$$\rho_3 = \frac{1}{3}\rho \begin{pmatrix} -\cos\phi\left(\cos\theta - \sqrt{2}\sin\theta\right) - \sqrt{6}\sin\phi \\ \sqrt{6}\cos\phi - \sin\phi\left(\cos\theta - \sqrt{2}\sin\theta\right) \\ \sqrt{2}\cos\theta + \sin\theta\cos\phi \end{pmatrix} \tag{3.43c}$$

$$\rho_4 = \frac{1}{3}\rho \begin{pmatrix} -\cos\theta\ \ \cos\phi + \sqrt{2}\cos\phi\ \ \sin\theta + \sqrt{6}\sin\phi \\ -\sqrt{6}\cos\phi - \sin\phi\left(\cos\theta - \sqrt{2}\sin\theta\right) \\ \sqrt{2}\cos\theta + \sin\theta\cos\phi \end{pmatrix} \tag{3.43d}$$

For a three-dimensional formation, there are 12 charged spacecraft equations of motions, 4 each for the $\hat{\mathbf{o}}_r$, $\hat{\mathbf{o}}_h$ and $\hat{\mathbf{o}}_\theta$ axes. The number of these equations can be reduced by applying the center of mass conditions and principal axes constraints. For a three-dimensional formation there are 3 center of mass constraints and 3 principal axes constraints, reducing the number of equations to be solved to 6. Applying the center of mass and principal axes constraint and using equations (2.6a)–(2.6c), the formation dynamics can be expressed in matrix form as

$$m \begin{bmatrix} 0 \\ 0 \\ 0 \\ z_1 \\ z_2 \\ -3x_1 \end{bmatrix} = \begin{bmatrix} \frac{y_1-y_2}{d_{12}^3} & \frac{y_1-y_3}{d_{13}^3} & \frac{y_1-y_4}{d_{14}^3} & 0 & 0 & 0 \\ \frac{y_2-y_1}{d_{12}^3} & 0 & 0 & \frac{y_2-y_3}{d_{23}^3} & \frac{y_2-y_4}{d_{24}^3} & 0 \\ 0 & \frac{y_3-y_1}{d_{13}^3} & 0 & \frac{y_3-y_2}{d_{23}^3} & 0 & \frac{y_3-y_4}{d_{34}^3} \\ \frac{z_1-z_2}{d_{12}^3} & \frac{z_1-z_3}{d_{13}^3} & \frac{z_1-z_4}{d_{14}^3} & 0 & 0 & 0 \\ \frac{z_2-z_1}{d_{12}^3} & 0 & 0 & \frac{z_2-z_3}{d_{23}^3} & \frac{z_2-z_4}{d_{24}^3} & 0 \\ \frac{x_1-x_2}{d_{12}^3} & \frac{x_1-x_3}{d_{13}^3} & \frac{x_1-x_4}{d_{14}^3} & 0 & 0 & 0 \end{bmatrix} \begin{bmatrix} \tilde{Q}_{12} \\ \tilde{Q}_{13} \\ \tilde{Q}_{14} \\ \tilde{Q}_{23} \\ \tilde{Q}_{24} \\ \tilde{Q}_{34} \end{bmatrix} \tag{3.44}$$

Equation 3.44 can be expressed in compact form using equation 3.2. The rank of matrix $\mathbf{A}$ is 6, thus it is a full rank matrix and a unique solution to $\tilde{\mathbf{Q}} = \mathbf{A}^{-1}\mathbf{x}$ is found. It is interesting to note that there is no null-space to exploit for a tetrahedron formation. There is only a

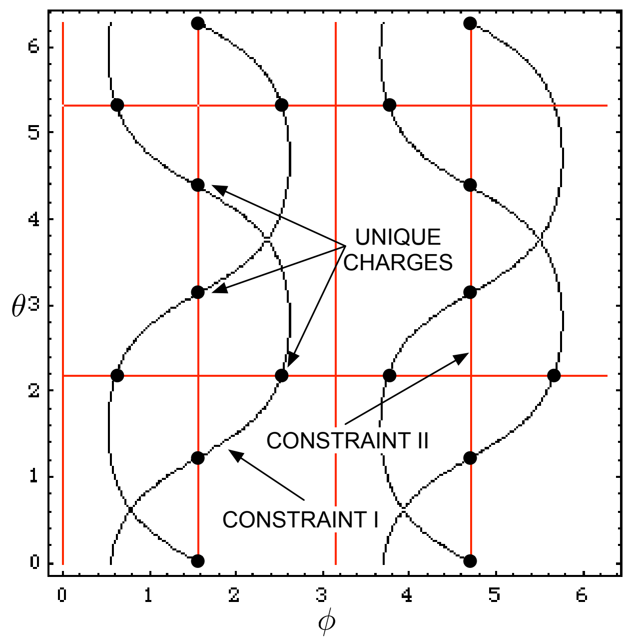

Figure 3.7: Orientation of Tetrahedron for unique charges for $\psi = 0$

unique set of charged products for the tetrahedron system expressed as

$$\mathbf{Q}^* = \frac{1}{9}m\rho^3 \begin{bmatrix} -4\sqrt{6}\left(3c^2\theta\ c^2\phi + \sqrt{2}c\theta\ s\theta\,(5+3c2\phi) - s^2\theta\right) \\ -\left(\sqrt{6}+5\sqrt{6}c2\theta + 6\sqrt{6}c^2\theta\ c2\phi - 2\sqrt{3}s2\theta\,(5+3c2\phi) + 36c\theta\ s2\phi\right) \\ -\left(\sqrt{6}+5\sqrt{6}c2\theta + 6\sqrt{6}c^2\theta\ c2\phi - 2\sqrt{3}s2\theta\,(5+3c2\phi) - 36c\theta\ s2\phi\right) \\ \sqrt{\frac{2}{3}}\left(-3-9c2\phi+5c2\theta\,(5+3c2\phi)+\sqrt{2}s2\theta\,(5+3c2\phi)+6\sqrt{6}c\theta\ s\phi + 24\sqrt{3}s\theta\ s2\phi\right) \\ \sqrt{\frac{2}{3}}\left(5c2\theta\,(5+3c2\phi)+\sqrt{2}s2\theta\,(5+3c2\phi)-3s2\phi\left(1+3c2\theta+2\sqrt{3}\left(\sqrt{2}c\theta+4s\theta\right)\right)\right) \\ -\sqrt{\frac{2}{3}}\left(33-45c2\phi+c2\theta\,(5+3c2\phi)+2\sqrt{2}s2\theta\,(5+3c2\phi)\right) \end{bmatrix} \tag{3.45}$$

Angles θ and ϕ are used to represent the orientation of the tetrahedron in space. The third angle ψ is set to 0° to simplify these algebraic expressions. The charged product solution depends on the orientation of tetrahedron vertex.

3.2.2 Unique Individual Charges

From equation 3.5 it is seen that the charged products for a planar formation depend on the null-space of the system. The null-space can be exploited to find specific charged products which result in unique spacecraft charges. For a three-dimensional formation there is only a unique set of charged products, which depend on the orientation of the tetrahedron in the space. This differentiates the analysis of a three-dimensional formation to that of a planar formation. The analysis presented here determines the conditions for unique spacecraft charges for ranges of three-dimensional tetrahedron attitudes.

A tetrahedron can be broken into triangular loops as shown in figure 3.2, focused on spacecraft position 1 to compute the charge on spacecraft 1. The charge on spacecraft 1 can be computed as shown by equations (3.8). For the planar formation the charged product solutions contains a 1-D null-space which yields infinity of potential $\tilde{Q}_{ij}$ solutions. By carefully choosing the value of the scaling parameter t it was shown that only one equality constraint from equation (3.8) is needed for unique spacecraft charges. With no null-space to exploit in a three-dimensional formation, the charge on spacecraft 1 $\tilde{q}_1$, should be unique to all the three loops in figure 3.2. Mathematically this condition can be represented as

$$\tilde{Q}_{12}\tilde{Q}_{34} - \tilde{Q}_{14}\tilde{Q}_{23} = 0 \tag{3.46a}$$

$$\tilde{Q}_{13}\tilde{Q}_{24} - \tilde{Q}_{14}\tilde{Q}_{23} = 0 \tag{3.46b}$$

For a planar square formation if one equality constraint is satisfied, the other constraint is guaranteed to be satisfied as well. For a three-dimensional formation there are two equality constraints that need to be satisfied for unique spacecraft charges. The conditions on ϕ and θ must satisfy the equality constraints in (3.46a) and (3.46b) to obtain a unique spacecraft charge $\tilde{q}_1$. Using equation 3.45, the equality constraints in (3.46) are written as

$$\frac{64}{27}m^2\rho^6\left(3c^2\phi - 2\sqrt{3}c\phi\ s\phi\left(\sqrt{2}c\theta + s\theta\right) + 3s\theta\ s^2\phi\left(2\sqrt{2}c\theta - s\theta\right)\right) = 0 \tag{3.47a}$$

$$\frac{256}{9}m^2\rho^6 c\phi\ s\phi\left(\sqrt{2}c\theta + s\theta\right) = 0 \tag{3.47b}$$

From equations (3.47a) and (3.47b), it is seen that regions where unique spacecraft charge exists are not intuitive. Figure 3.7 presents the contour plots for the equality constraints in equations (3.47a) and (3.47b). Equation (3.47a) in figure 3.7 corresponds to constraint I and equation (3.47b) is represented by constraint II. The regions of unique charges are indicated by the points of intersection of two equality constraints. It is evident from figure 3.7 that unique charges on a tetrahedron exist for $\phi = 90°$ or $\phi = 270°$. Such an orientation corresponds to the vertex of the tetrahedron aligned with the $\hat{\mathbf{o}}_\theta$ direction, and the remaining spacecraft form an equilateral triangle in $\hat{\mathbf{o}}_r$-$\hat{\mathbf{o}}_h$ plane. The spacecraft 1 is aligned with $\hat{\mathbf{o}}_\theta$ axis for $\phi = 90°$ or $\phi = 270°$ only if $\psi = 0°$. Unique charges also do exist for other tetrahedron orientations, where the spacecraft is not aligned along $\hat{\mathbf{o}}_\theta$ axis.

3.2.3 Real Spacecraft Charges

As in case of a planar formations, finding the regions where the uniqueness conditions are satisfied is not sufficient for a virtual Coulomb structure. The individual charges on a spacecraft should also be real. The mathematical conditions for real charges used for planar formations in equation (3.31) are used for the tetrahedron formation. The inequality constraints in (3.31) imply that for each of the loops in the tetrahedron the individual spacecraft should be real. It was noted that for a four-craft formation, if a unique charge $\tilde{q}_1$ exists, only one inequality constraint in equation (3.31) needs to be satisfied. Figure 3.8 shows the contour plot of the inequality constraint for real charges in equation (3.31a)

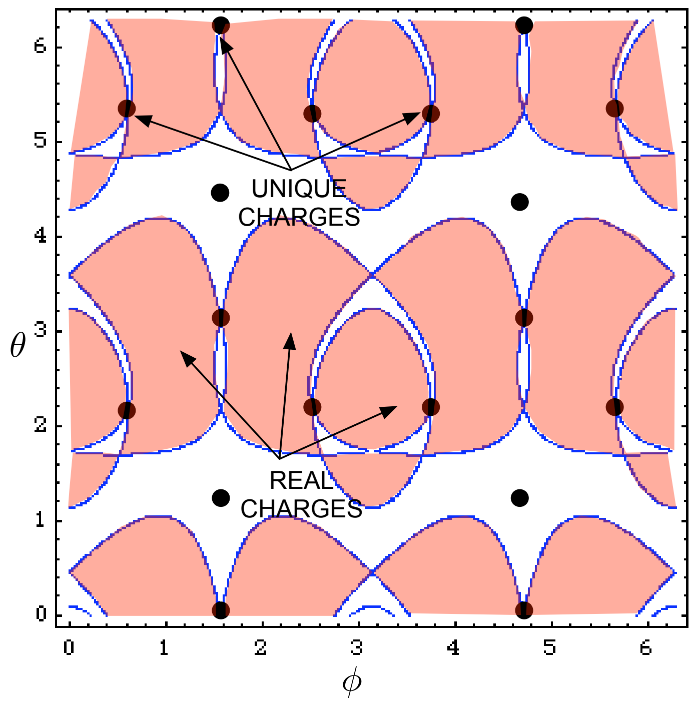

Figure 3.8: Orientation of Tetrahedron for real charges for $\psi = 0$

From figure 3.8 is it seen that individual charge $\tilde{q}_1$ on spacecraft 1 is real while the spacecraft is aligned with the $\hat{\mathbf{o}}_\theta$ axis. It is also seen that real charges are possible for orientations other than $\phi = 90°$ or $\phi = 270°$. Such orientations lie on the contours of the inequality constraint. This implies that the inequality constraint in equation (3.31a) is equal to 0 and one of the spacecraft charges is also 0. Thus the tetrahedron formation is reduced to a 3-craft equilateral triangle in $\hat{\mathbf{o}}_r$- $\hat{\mathbf{o}}_h$ plane. The analytic solution for the 3-craft formation is developed rigorously in reference 28.

The analysis presented here assumes that $\psi = 0°$. Figure 3.10 shows the conditions for real and unique spacecraft charges on ϕ and θ, for different values of ψ. From the figure 3.10 it is seen that orientations for unique charges are only possible when the inequality constraint in equation (3.31a) is equal to 0. This implies one of the spacecraft charges is 0, and the formation simplifies to a 3-craft equilateral triangle formation. Figure 3.9 shows one example of a possible orientation of the tetrahedron in space. The body frame orientation is expressed with respect to the Hill frame by rotation angles $\phi = 90°$, $\theta = 0°$ and $\psi = 0°$.

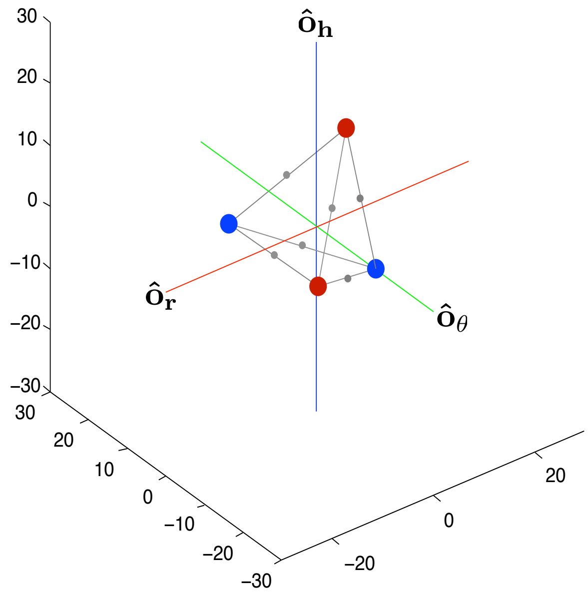

Figure 3.9: Potential Coulomb structure in shape of Tetrahedron

The analysis of the three-dimensional tetrahedron formation presented here assumed that the spacecraft have equal masses. It is however possible to have a tetrahedron formation oriented arbitrarily in space with variable mass. Analysis of the tetrahedron formation with variable mass needs to be addressed by future research work.

3.3 Co-Linear Formations

A linear four-craft formation aligns the spacecraft along one of the Hill frame axes. Formations aligned along $\hat{\mathbf{o}}_\theta$ are naturally occurring solutions and do not need any charging. For the analysis presented here, formation along $\hat{\mathbf{o}}_\theta$ will not be considered. The center of mass condition in a linear formation can be realized by carefully placing the spacecraft along the Hill frame axes. The principal axes constraint is implicitly satisfied when the spacecraft are placed on the Hill frame axes.

3.3.1 Three-Dimensional Null Space for Co-Linear Formations

Figure 3.11 presents a co-linear formation aligned with $\hat{\mathbf{o}}_r$ axis. The position vector of the

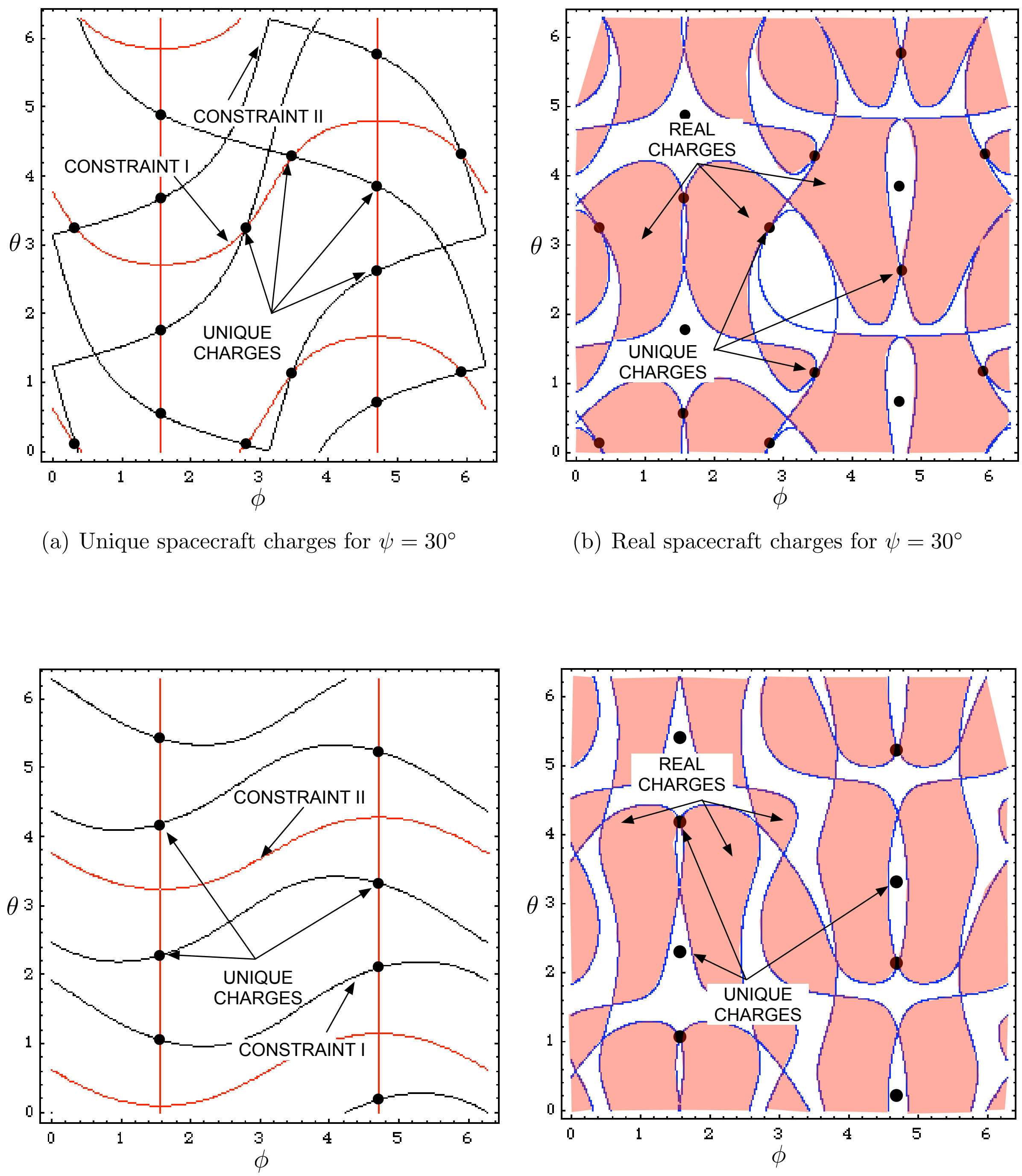

(a) Unique spacecraft charges for $\psi = 30^\circ$

(b) Real spacecraft charges for $\psi = 30^\circ$

(c) Unique spacecraft charges for $\psi = 60^\circ$

(d) Real spacecraft charges for $\psi = 60^\circ$

Figure 3.10: Range of θ and ϕ for real and unique spacecraft charges

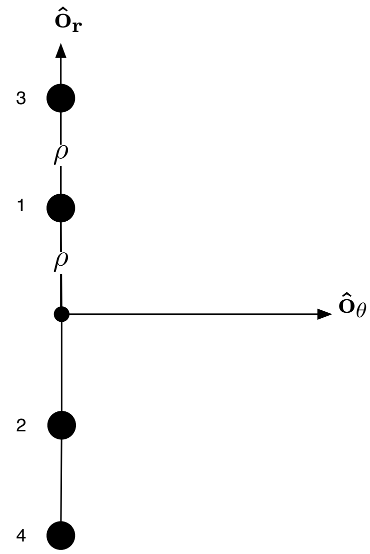

Figure 3.11: Linear formation aligned along $\hat{\mathbf{o}}_r$ axes

formation in Hill frame coordinates is expressed as

$$\boldsymbol{\rho}_1 = \begin{pmatrix} \rho \\ 0 \\ 0 \end{pmatrix}, \; \boldsymbol{\rho}_2 = \begin{pmatrix} -\rho \\ 0 \\ 0 \end{pmatrix}, \; \boldsymbol{\rho}_3 = \begin{pmatrix} 2\rho \\ 0 \\ 0 \end{pmatrix}, \; \boldsymbol{\rho}_4 = \begin{pmatrix} -2\rho \\ 0 \\ 0 \end{pmatrix}$$

For a co-linear formation, there are 4 charged equations of motion. The number of equations can be reduced by applying the center of mass condition and principal axes constraints. For a co-linear formation there is only 1 center of mass constraint and no principal axes constraint, as the formation is aligned with the Hill frame axis. The number of equations reduces to 3. Using equations (2.6a)−(2.6c), the formation dynamics along $\hat{\mathbf{o}}_r$ is expressed in matrix form as

$$-3m \begin{bmatrix} x_1 \\ x_2 \\ x_3 \end{bmatrix} = \begin{bmatrix} \frac{x_1-x_2}{d_{12}^3} & \frac{x_1-x_3}{d_{13}^3} & \frac{x_1-x_4}{d_{14}^3} & 0 & 0 & 0 \\ \frac{x_2-x_1}{d_{12}^3} & 0 & 0 & \frac{x_2-x_3}{d_{23}^3} & \frac{x_2-x_4}{d_{24}^3} & 0 \\ 0 & \frac{x_3-x_1}{d_{13}^3} & 0 & \frac{x_3-x_2}{d_{23}^3} & 0 & \frac{x_3-x_4}{d_{34}^3} \end{bmatrix} \begin{bmatrix} \tilde{Q}_{12} \\ \tilde{Q}_{13} \\ \tilde{Q}_{14} \\ \tilde{Q}_{23} \\ \tilde{Q}_{24} \\ \tilde{Q}_{34} \end{bmatrix} \tag{3.48}$$

Here $d_{ij} = |x_j - x_i|$. Equation (3.48) can be expressed in terms of ρ as

$$-3m\rho^3 \begin{bmatrix} 1 \\ -1 \\ 2 \end{bmatrix} = \begin{bmatrix} \frac{1}{\sqrt{2}} & -1 & \frac{1}{\sqrt{3}} & 0 & 0 & 0 \\ -\frac{1}{\sqrt{2}} & 0 & 0 & -\frac{1}{\sqrt{3}} & \frac{1}{\sqrt{2}} & 0 \\ 0 & 1 & 0 & \frac{1}{\sqrt{3}} & 0 & \frac{1}{2} \end{bmatrix} \begin{bmatrix} \tilde{Q}_{12} \\ \tilde{Q}_{13} \\ \tilde{Q}_{14} \\ \tilde{Q}_{23} \\ \tilde{Q}_{24} \\ \tilde{Q}_{34} \end{bmatrix} \tag{3.49}$$

The matrix $\mathbf{A}$ does not depend on the axes in which the formation is aligned. Thus it is constant whether the formation is aligned along $\hat{\mathbf{o}}_r$ or $\hat{\mathbf{o}}_h$ axes. The null-space of the system defined by $\mathbf{A}$ is also constant and does not vary with the axes in which formation is aligned. To determine the individual charges on spacecraft knowledge of charged products for the formation is necessary. The rank of matrix $\mathbf{A}$ is 3, and there are infinitely many solutions to $\tilde{\mathbf{Q}}$. The charged product solutions can be expressed in terms of the null-space of the system and the least squares solution to equation (3.49). The null space of the system described in (3.48) is written as

$$Q_{\text{null}} = \begin{bmatrix} 0 & 4 & -\frac{4}{9} \\ -\frac{1}{16} & 0 & -\frac{1}{9} \\ -\frac{9}{16} & -9 & 0 \\ 0 & 0 & 1 \\ 0 & 1 & 0 \\ 1 & 0 & 0 \end{bmatrix} \tag{3.50}$$

The least squares solution for the system described by (3.49) is expressed using equation (3.4). Using equation (3.5), all the possible solutions for $\tilde{\mathbf{Q}}$ are expressed as

$$\tilde{\mathbf{Q}} = \mathbf{Q}^* + t_1\mathbf{Q}_{\text{n}1} + t_2\mathbf{Q}_{\text{n}2} + t_3\mathbf{Q}_{\text{n}3} \tag{3.51}$$

Here $\mathbf{Q}_{\text{n}i}$ represents each column of the null space given in equation (3.50), and t_i is parameter used to scale the column vector of the null space. For the system given by equation (3.48) the least squares solution is

$$Q^* = -\frac{m\rho^3}{15329} \begin{bmatrix} 372684 \\ 66408 \\ 173016 \\ 173016 \\ 66408 \\ 372684 \end{bmatrix} \tag{3.52}$$

The least squares inverse solution is not independent of the axes of orientation. The least squares inverse solution in equation 3.52 is for a linear formation aligned along $\hat{\mathbf{o}}_r$ axis. Similar analysis can be performed for $\hat{\mathbf{o}}_h$ axis to determine the charged products for relative equilibrium. The next section discusses methods to calculate the individual spacecraft charges from the charges product obtained in equation (3.51).

3.3.2 Unique Individual Spacecraft Charges

Finding individual charges is not a trivial process, as only 4 individual charges are needed, but we have 6 charged products. To solve for $\tilde{q}_1$, we can break up the formation into 3 different loops about the spacecraft position 1 similar to figure 3.2. Charge $\tilde{q}_1$ can be calculated as defined by equation (3.8). The equality constraints for unique charges is written as

$$\tilde{Q}_{12}\tilde{Q}_{34} - \tilde{Q}_{13}\tilde{Q}_{24} = 0 \tag{3.53a}$$

$$\tilde{Q}_{12}\tilde{Q}_{34} - \tilde{Q}_{14}\tilde{Q}_{23} = 0 \tag{3.53b}$$

For a planar square formation the number of equality constraints can be reduced by carefully choosing the null-space scaling factor. With a 1-D null-space for planar formations, it is easy to determine the regions for unique individual charges by solving a quadratic polynomial equation. Linear formations on the other hand have three-dimensional null-space. Figure 3.12(a) presents a three-dimensional surface plot of the first equality constraint in equation (3.53a) as function of the scalar parameter t_i. The region where the equality constraint is satisfied is represented by shaded region.

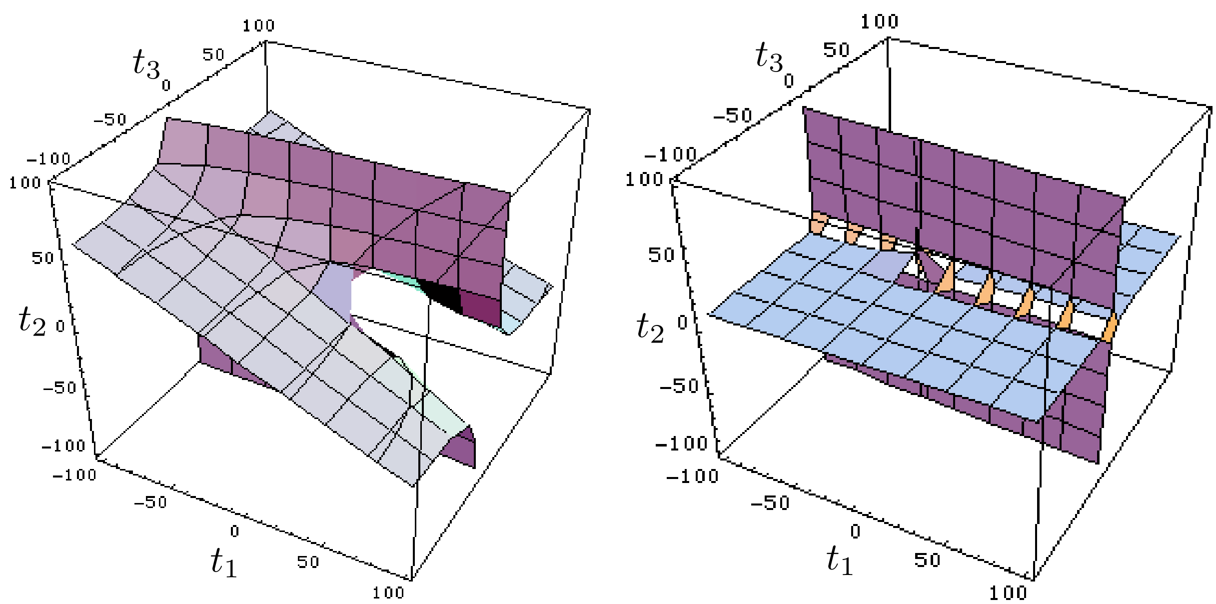

(a) Plot of equality constraint in equation (3.53a) (b) Plot of equality constraint in equation (3.53a)

Figure 3.12: Contour plot of equality constraint for unique spacecraft charges

It is noted from figure 3.12(a) that regions where equality constraints are satisfied are quite complex. For a unique spacecraft charge, this is not a sufficient condition. The equality constraint in equation (3.53b) also must be satisfied. Figure 3.12(b) presents the three-dimensional surface plot of the equality constraint in (3.53b). It can be seen that the regions of intersection between the plots in figures 3.12(a) and 3.12(b) are not intuitively obvious. The complexity of determining regions of unique spacecraft charges increase as the null-space dimension of the system increases. The analysis presented for the linear formation serves as an open question on how to compute spacecraft charges for systems with null-space dimension higher than 1. The results for a linear four-craft formation have not yet been developed. The steps are developed to show the complex nature of the analysis. It is interesting to note that the numerical solutions have never shown a 1-D four-craft formation.

Chapter 4

Distributed Computing Tool for Static Coulomb Formations

Determining the possible shapes of a Coulomb virtual structure is a non-intuitive process because of the complex interactions between Coulomb forces and relative motion dynamics. Applying the center of mass condition and the principal axes constraints reduces the number of potential solutions. The center of mass and principal axes constraints are only necessary and not a sufficient condition for a static formation to exist. For a large number of spacecraft in a formation, it is not possible to determine all the possible formation shapes even after applying the constraints for center of mass and principal axes. Hence the need for numerical tools to determine all the potential solutions. Numerical tools are also useful for verifying the analytic solutions.

This chapter presents the use of a distributed Genetic Algorithms (GA's) as a tool for the numerical analysis of the Coulomb virtual structure. The GA's are based on the Darwinian principle of the survival of the fittest, where the fittest members of a population survive and are allowed to reproduce. First, a brief introduction to a single processor GA is presented as it serves as foundation for a distributed GA. The GA's are increasingly being used in optimization problems. In aerospace applications the GA's have been applied to missions such as low-thrust optimal trajectories[8] and structure shape control.[10]

Traditional gradient based optimization methods require an initial guess to the optimization problem. The gradient based method also restricts the search space to a local region around the initial guess. The GA's avoid both these problem as it does not require an initial guess to the problem. The search space is also not restricted to the region around the starting value. The drawback of using a GA is the large amount of computation time required to arrive at a solution. The computation time can be reduced by distributing the work GA does over several processors. This is achieved by dividing the overall population into smaller groups or sub-populations. This reduces the computation time required by each individual processors, thus reducing the overall computation time required for the optimization problem.

After the discussion of a single processor, the implementation of the distributed GA is presented. This chapter also discusses issues with cost function and load balancing, and how to over come these problems. The results of distributed GA concludes the chapter.

4.1 Single Processor Genetic Algorithm

The implementation of a single processor GA serves as the foundation for a distributed GA. An optimization problem involves minimizing a cost function $\mathcal{J}(\mathbf{p})$ with respect to parameters $\mathbf{p}$. The gradient based method begins with an initial guess for the parameters $\mathbf{p}$, and then searches in the direction of steepest descent $\partial\mathcal{J}/\partial\mathbf{p}$ to find the local minimum. The gradient based method is not the ideal method to use in optimization problems such as solution to static Coulomb formation as the initial guess for such a problem is not intuitively obvious. The GA's are able to overcome the difficulties of the gradient based method as it does not approach the solution from one direction and avoids the non-optimal minima's and discontinuities in the cost function.

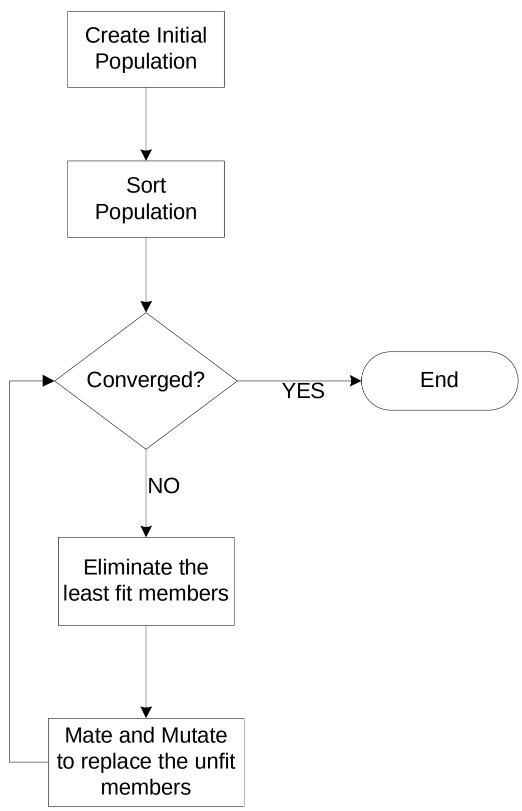

Figure 4.1: Implementation of a Single Processor Genetic Algorithm

The set of parameters that characterize an individual member in a population vary according to the problem. These parameters are analogous to genes in the biological world. Each member of a population is a potential solution to the static Coulomb formation problem. The parameters characterizing each member include the relative x, y and z positions of each spacecraft in a formation along with the charge $\tilde{q}$ on each satellite. Figure 4.1 illustrates a basic implementation of a single processor GA. The GA initially creates a random population. The fitness of each member of the population is evaluated using the cost function $\mathcal{J}(\mathbf{p})$. The discussion of how to find a good cost function for the static Coulomb formation search is tackled in a later section. Each member in the population is constrained so that it satisfies the center of mass and the principal axes constraint.

Each member of the population is sorted according to their fitness, from the most fit to the least fit. The least fit members are then eliminated, and the remaining fit members are allowed to mate to replace the unfit members. The percentage of unfit members eliminated is a user defined property, and for the analysis presented in this chapter only the top 30% of the population are allowed to survive and reproduce. The population is again sorted. This process of sorting and eliminating the unfit members, and mating continues until the GA converges to a solution. The sequence of sorting, elimination and mating represents a generation of evolution in the GA. The convergence of the GA is determined by the fitness of the most-fit member of the population. If the fitness of the most-fit member reaches a specified tolerance, the GA is said to have converged.

Mating of the fittest members of the population to generate child members, represents a recombination of the parent's parameters. The mating process used in the GA for the analysis is described in detail by Berryman in reference 28. The mating process determines how the population evolves over time and thus the rate of convergence to the solution. The mathematical expression describing the mating process is represented as follows[28]

$$p_{i_{child}} = w_i p_{i_{father}} + (1 - w_i)\, p_{i_{mother}} \tag{4.1}$$

Where w_i is the weighting average and determines which of the methods described in reference 20 is used. The algorithm uses two methods to mate parents to generate offspring's. The first method creates a child member from either of the parent member, and the weighting average is either 0 or 1. The second method used for mating interpolated to a point about the parents. To allow the GA to search in areas beyond the area defined by parents, the weighting average is allowed to go beyond 0%/100% ratio. The frequency of the method used to mate is randomly decided by the algorithm.[28]

While mating allows the population to evolve over time, the whole search space is not explored. Even after allowing for the weighting average to go beyond 0 and 1, the search space is not fully explored. Random mutation of the child members allows the GA to explore the search space not spanned by the parent members. Mutation is allowed to occur in one of the parameters chosen randomly. Mutation can occur either in the position of the spacecraft or the charge required on the spacecraft. The mathematical expression for the mutation process is represented as follows[28]

$$p_i = p_i + M_i \tag{4.2}$$

M_i is the mutation factor used to mutate the parameter. Not every child member is mutated, but only a randomly selected number of child members are mutated. Once it is determined which child members are to be mutated, the GA randomly determines which parameter to mutate. The child members are also constrained to make sure they satisfy the principal axes and the center of mass constraint. Also the child members whose parameters value fall outside the pre-defined search space are ignored.

4.2 Distributed Genetic Algorithm

A drawback of using the GA's is the large amount of computation time required to arrive at a potential solution. The mating, mutation and sorting of a large population size can significantly slow down the computation. The difficulty of computation time can be overcome by breaking down the overall population size into smaller subsets and allowing each subset to evolve over time separately. Each individual processor is assigned a subset of the population, reducing the computation time required by each processor and speeding up the overall process. This method of distributing the work over several different processors is known as parallel processing.

In the process of natural evolution, the traits of the fittest member of the population tend to dominate the population. Along similar lines in the GA, the characteristics of the fittest member of the population tend to dominate and solution tends to converge to a local minimum. Distributing the population into smaller subsets and allowing migration to occur among the subset population, the issue of convergence to local minimum is avoided.[11]

This section presents the basic implementation of the distributed GA used in the analysis. This section also addresses some of the issues associated with distributed GA such as cost function definition and load balancing. Finally the section also compares the performance of distributing the work load over several different processors.

4.2.1 Implementation

In a distributed genetic algorithm the population is divided into smaller sub-population sets and allowed to evolve separately. The population from each individual processor is allowed to migrate to allow the solution to converge to the global minimum. There are many protocols which allow for communication between individual processors. For the distributed GA analysis presented here the Message Passing Interface (MPI) protocol was used. A 'master-slave' implementation of MPI is used in the distributed GA for distributing the work among different processors. The master node monitors the progress of slave nodes and distributes the work among slave nodes. The master node also maintains a master population, which is a collection of the fittest members found by the solution. Figure 4.2 illustrates the 'master-slave' implementation of the MPI protocol.

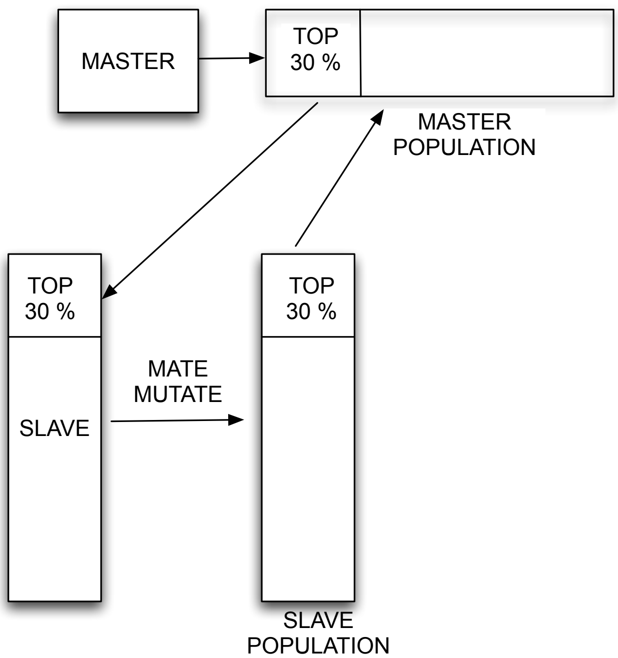

Figure 4.2: Master-Slave implementation of the Message Passing Interface protocol)

Figure 4.3 illustrates the implementation of the distributed GA presented here. The master node distributes the population among the slave nodes. Migration of population between slave nodes occur via the master node, as slave nodes do not communicate directly with each other. Each slave node receives a set of population from the master node. The population received by slave node is pre-sorted and the least fit members are already eliminated. The initial population set received by the slave node is different from the master population. This is done to ensure that the whole search space is explored.

The slave node then mates and mutates the fit members to replenish the unfit members. The master then receives the fit members of the sorted slave population. The fit members are integrated into the existing master population and the population resorted. The slave henceforth only receives the members from the master population and this process continues until the GA converges. An iteration when each slave node has communicated with the master node once is called a generation in the distributed GA. The mating and mutation processes to replenish the population is the same process as used by a single processor GA. The distributed GA is essentially several different single processor GA's controlled by a single master node. Here the work of one processor is divided into several processors creating the distributed effect.

The GA is said to have converged when the fittest member of the master population reaches a specified tolerance. The fitness of each member of population is evaluated by a cost function. The cost function plays an important role in GA as it determines whether a solution has been found by GA.

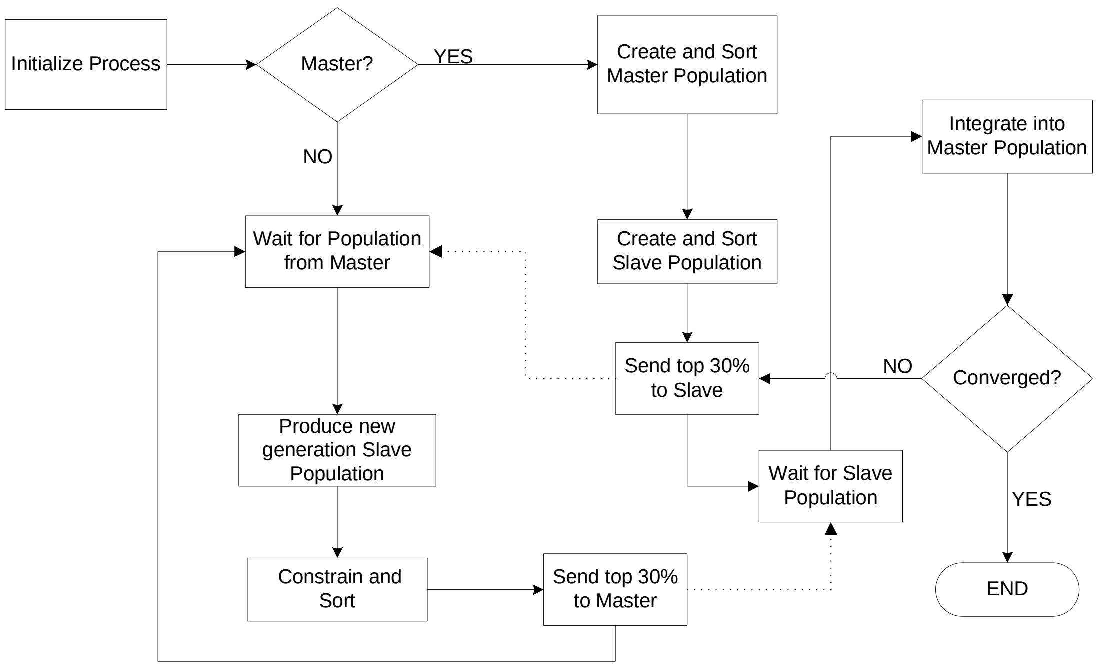

Figure 4.3: Implementation of distributed Genetic Algorithm (GA)

4.2.2 Cost Function

GA's are optimization tools which search for a set of parameters that minimize a given cost function. There are many choices for a cost function that can be used to optimally find the solution for the static Coulomb formation problem. In determining solutions to the static Coulomb formation. The charges on a spacecraft are desired such that they exactly cancel out the acceleration experienced by the spacecraft in the Hill frame. The most intuitive fitness function, which has physical meaning, is the total Hill frame acceleration of the formation[28]

$$J(\rho) = \sum_{i=1}^{N} \|\ddot{\rho}_i\| \tag{4.3}$$

where

$$\ddot{\rho}_i = \ddot{\rho}_{\mathcal{H}_i} + \sum_{j=1}^{N} \ddot{\rho}_{ij} \tag{4.4}$$

$$\ddot{\rho}_{ij} = \frac{1}{m_i} \frac{\rho_i - \rho_j}{|\rho_i - \rho_j|^3} \tilde{q}_i \tilde{q}_j \tag{4.5}$$

$$\ddot{\rho}_{\mathcal{H}_i} = \begin{pmatrix} -3x_i \\ 0 \\ z_i \end{pmatrix} \tag{4.6}$$

Here $\ddot{\rho}_{H_i}$ is the acceleration experienced by the spacecraft when it is placed in the Hill frame with no initial velocity and no charges are acting on it. Although this cost function has physical meaning, the drawback of using this cost function is that it always leads to trivial solutions. Here the spacecraft are aligned in the along-track direction and have no charge. This solution occurs as any satellite aligned in along track direction does not experience acceleration in Hill frame. Thus the formation does not need Coulomb interaction between the spacecraft. To overcome this problem another cost function was developed. The new fitness function was cost function in equation (4.3) weighted by Coulomb interaction between the satellites.[28]

$$J(\rho) = \frac{\sum_{i=1}^{N} \|\ddot{\rho}_i\|}{\sum_{j=1}^{N} \sum_{i=1}^{N} \|\ddot{\rho}_{ij}\|} \tag{4.7}$$

This cost function avoids the trivial solutions by penalizing possible formations as they approach the trivial solution, thus leading to non-trivial formations. A drawback of this cost function is that it has no physical meaning. The fitness of the formation is determined by evaluating the cost function. The solution is said to have converged once the fitness of the best member of the population reaches a certain specified tolerance. It is not intuitively obvious what the specified tolerance needs to be for convergence to a potential solution. To overcome this drawback a cost function with more physical significance is used in the GA. A candidate fitness function is developed by weighing the cost function in equation (4.3) by the Hill frame acceleration $\ddot{\rho}_{H_i}$.

$$J(\rho) = \frac{\|\ddot{\rho}_i\|_\infty}{\|\ddot{\rho}_{\mathcal{H}_i}\|_\infty} \tag{4.8}$$

The physical meaning of the cost function is that it gives the ratio of total acceleration of the satellite to the Hill frame acceleration it would experience if no charges were acting on the satellite. This cost function also avoids GA converging to trivial solution by penalizing formations as they approach the trivial solution.

4.2.3 Load Balancing

For a distributed GA with the 'master-slave' MPI implementation to work efficiently, the master node should be distributing work evenly. The master node should be idle while waiting for communication from the slave nodes. The slave nodes should constantly be working and not be idle. The master node just acts as an interface for allowing migration of the fittest members of one sub-population to another. The distributed GA should work efficiently, as the master node for the most part is only waiting for information from the slave nodes. Figures 4.4 and 4.5 show the load balancing pattern of the distributed GA.

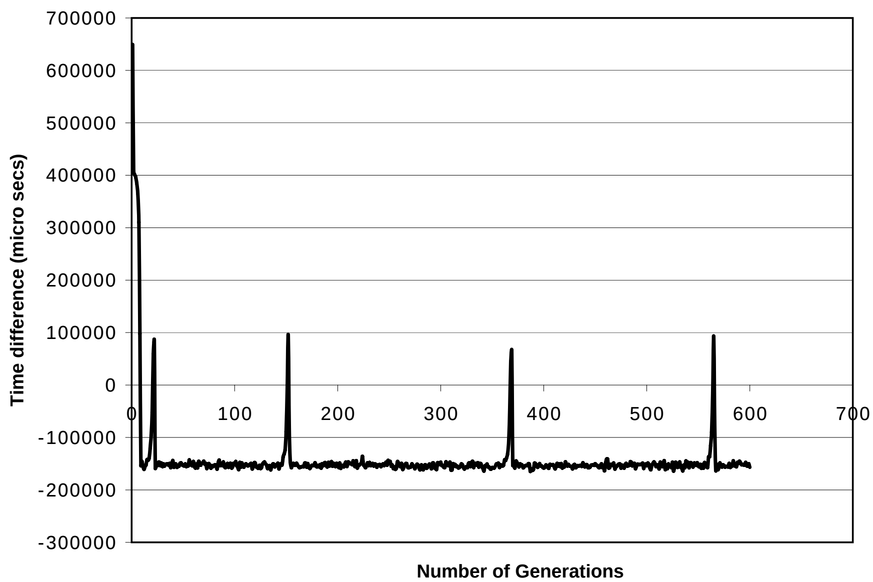

Figure 4.4: Time difference between Master and Slave for a regular population size

Figure 4.4 shows the difference in waiting times for master and slave nodes. The size of the population set received by each slave node is a 1000 members. The master node is waiting for communication from the slave node. The time taken by the slave node to complete its task and send communication back to the master node is called the master waiting time. The slave waiting time is the amount of time it takes for the master node to send communication back to the slave node. The time difference is computed by subtracting the master waiting time from the slave waiting time. A negative time difference indicates that master node is waiting for communication and slave node is doing the work. Figure 4.5 shows the difference in waiting times for master and slave nodes for a population size of 100 members. From the figure 4.4 we see that GA works efficiently as the master node is waiting for communication, and the slave node is constantly working, which makes the distributed GA efficient. Increasing the number of members in a population increases the workload of slave nodes, making the 'master-slave' implementation efficient.

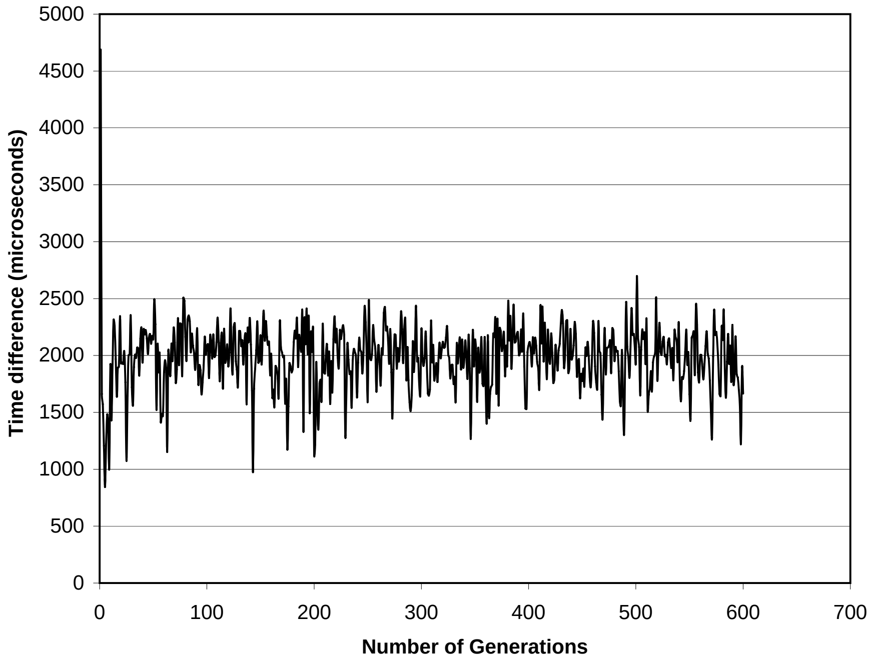

Figure 4.5: Time difference between Master and Slave for a reduced population size

4.2.4 Performance of the distributed GA

This section presents some of the results of performance of the distributed GA used in the analysis here. Figure 4.6(a) presents the plot of fitness vs. generation for 2 slave nodes. Figure 4.6(a) illustrates that each run of the GA is statistically different from another, and convergence rates of the GA vary for each run.

If the population size is fixed for a node, the distributed GA on average should converge to better fitness values as the number of nodes are increased. Figure 4.6(b) shows the averaged run of the distributed GA for 2, 3 and 5 nodes. The fitness values are averaged over 10 runs. For N number of nodes, there is always 1 master node and N-1 number of slave nodes. Increasing the number of slave nodes implies that the overall population size is increased. Increasing the overall population size for the GA leads to better fitness convergence rates. This trend is illustrated in figure 4.6(b), where increasing the number of slave nodes, the GA converges at a faster rate.

Increasing the overall population size of the GA allows it to converge to a fitter solution. Running the GA across one node, and increasing the population size for that node, would result in better convergence of the GA. This raises the question, why use the distributed GA? The amount of computation time can be reduced by distributing the overall population into smaller subsets across several different slave nodes. Figure 4.7 shows the average com-

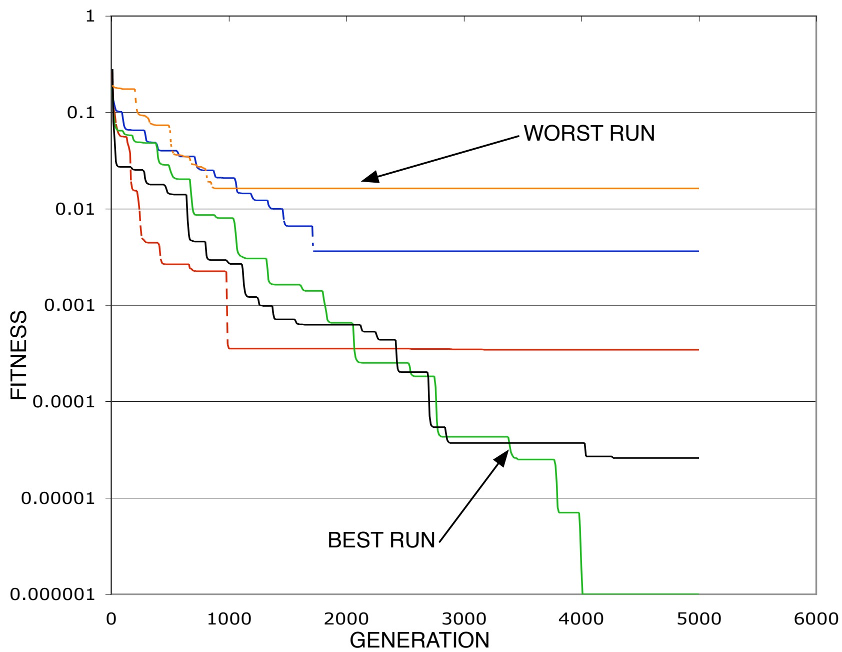

(a) Distributed GA run over a 2 slave nodes

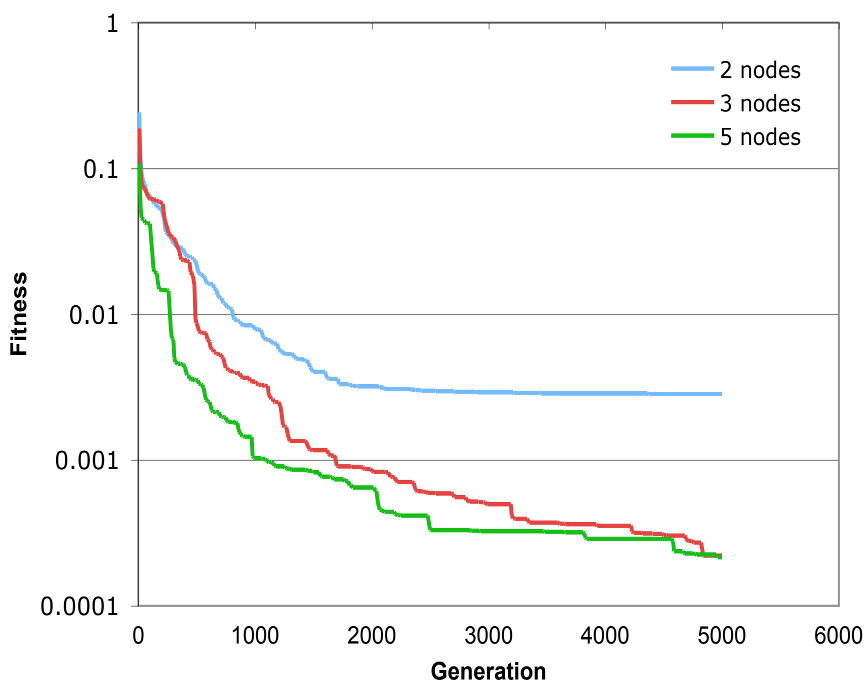

(b) Distributed GA run for different nodes averaged over 10 runs

Figure 4.6: Performance analysis of the distributed GA

putation time required to reach a convergence criteria for different number of slave nodes. The computation time for each node was averaged over 5 runs. Here the overall population size was kept constant. For each run, the population size of the slave node was calculated by dividing the overall population size by the total number of slave nodes. For a given number of nodes the error bars represent the the range of computation time.

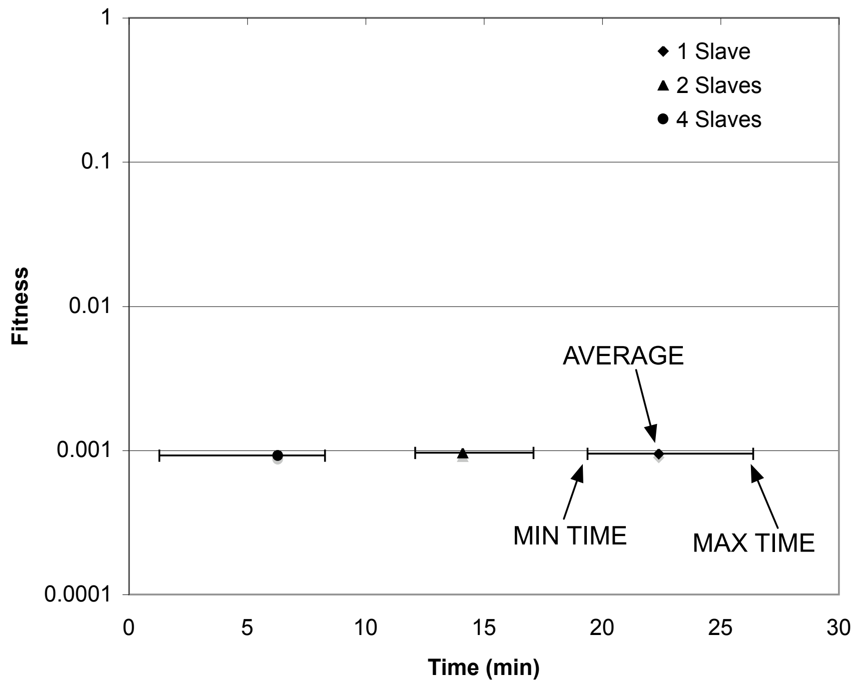

Figure 4.7: Average computation time analysis for the distributed GA averaged over 5 runs

Increasing the number of nodes and reducing the population size received by each node reduces the computation time. From figure 4.7 it is observed that a distributed GA significantly reduces the computation time as compared to a single processor GA. This analysis validates the usefulness of the distributed GA as a tool for finding solutions to static Coulomb formations.

4.3 Numerical Results

This section presents some of the results of the numerical analysis described in this chapter. The static formations found by the distributed GA are not the exact solution to the Coulomb formation problem described in chapter 2. The candidate solutions found by the GA serve as an initial guess for use in gradient based optimization methods. The formations presented here are unique as compared to the formations presented in references 28 and 12. The formations presented here have constant and equal spacecraft mass. The GA presented in references 28 and 12, was allowed to vary the spacecraft mass to find a candidate formation.

The GA is allowed to run until the convergence criteria is met. Once the fitness of the first member of the integrated master population reached a certain tolerance level, the GA was said to have converged. The tolerance limit specified for the convergence of GA is 0.001. Referring back to the discussion of cost function earlier in the chapter, the final Hill frame acceleration of the spacecraft is reduced by a factor of 1000. The final Hill frame acceleration of the spacecraft refers to the acceleration experienced by spacecraft in the rotating Hill frame, while the spacecraft is charged.

Figure 4.8 presents some of the Coulomb structure shapes arrived at by the distributed GA. The $\hat{\mathbf{o}}_r$, $\hat{\mathbf{o}}_h$ and $\hat{\mathbf{o}}_\theta$ are the rotating Hill frame axes. For these virtual structures it is verified that the center of mass and principal constraints are satisfied. Figure 4.8(a) is a planar 4-craft formation. Here 3 craft are aligned co-linearly and the fourth craft is positioned in a manner such that the structure resembles a triangle. A 3-D structure resembling a tetrahedron is shown in figure 4.8(b). The structure is not a pure tetrahedron as it is not made up of equilateral triangles.

The analysis in chapter 3 predicted that a 3-D tetrahedron like structure only exists when the vertex is aligned along $\hat{\mathbf{o}}_\theta$ axis. The 3-D structure found by the GA validates this analysis. The Coulomb structure found by the GA is not a pure tetrahedron and can be oriented in an arbitrary fashion. A 5-craft Coulomb structure found by the GA is shown in figure 4.8(c). Here four spacecraft form a planar structure in the $\hat{\mathbf{o}}_r$-$\hat{\mathbf{o}}_h$ plane, and the fifth craft is placed along $\hat{\mathbf{o}}_\theta$ axis to complete a 3-D structure. This 5-craft formation is a potential mission for applications such as interferometry.

Spacecraft formations with similar shape as figure 4.8(c) are found for 6 and 10-craft formations. Figure 4.8(d) shows a 6-craft formation. Here three spacecraft are aligned along $\hat{\mathbf{o}}_\theta$ axis and the remaining three spacecraft are aligned in a triangular shape to complete the formation. Figure 4.9 shows a 10-craft formation. Here nine spacecraft are aligned in $\hat{\mathbf{o}}_h$-$\hat{\mathbf{o}}_\theta$ plane and one spacecraft is aligned along $\hat{\mathbf{o}}_r$ axis to complete the 3-D formation.

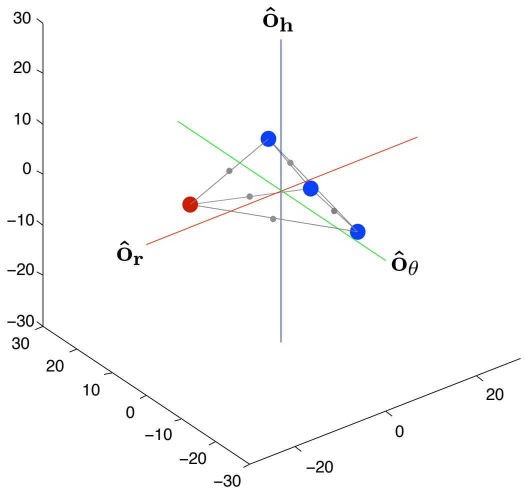

(a) 4-Craft Formation

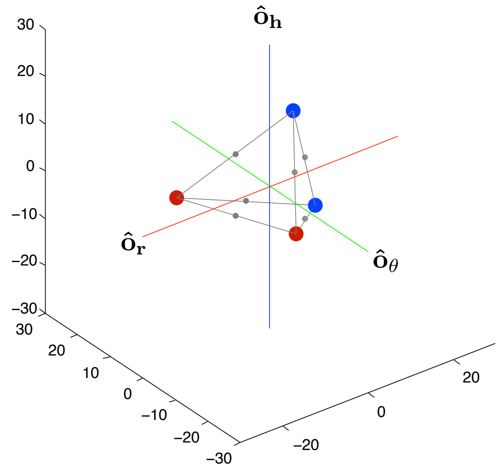

(b) 4-Craft Formation

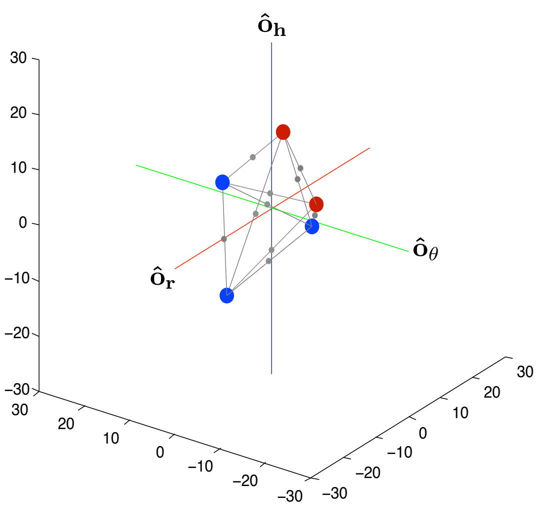

(c) 5-Craft Formation

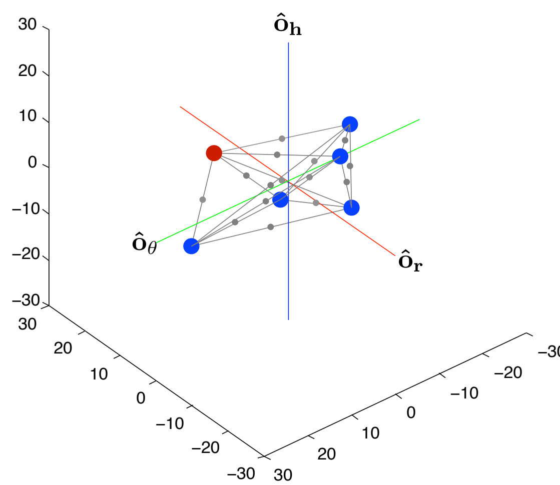

(d) 6-Craft Formation

Figure 4.8: Coulomb Virtual Structure Solutions determined by the GA

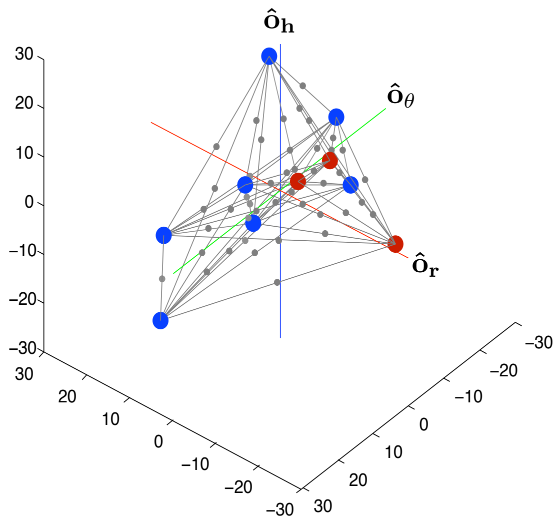

Figure 4.9: 10-Craft Coulomb Virtual Structure Solution determined by the GA

Chapter 5

Conclusions and Future Work

Using multiple spacecraft to form a smaller formation is gaining increasing popularity over large monolithic structures. Coulomb propulsion offers an attractive solution as a controller in close proximity spacecraft formations. Coulomb propulsion has no thruster exhaust and no damage occurs to spacecraft in close proximity. Coulomb thrusting also has the advantages of being essentially propellant-less and massless.

This thesis presents the use of Coulomb propulsion in a static spacecraft formation. Analytical and numerical tools for determining the solution to static formation are discussed. Analytic solutions extend the work done on 2 and 3-craft formation and present an analysis on a 4-craft formation. For a 4-craft formation the issue of unique spacecraft charges arises for the first time.

The thesis discusses a square Coulomb structure for a planar 4-craft formation. The square formation was parameterized in terms of the radius ρ and orientation angle θ for any given plane. The range of angle θ where unique and real spacecraft charges exist are identified. The thesis also presents the criteria for computing unique and real spacecraft charges. For a planar formation, the charged products are a function of the null-space. By carefully choosing the null-space scaling parameter, the equality constraints for unique spacecraft charges is reduced. The solutions to the individual spacecraft charges is provided.

The thesis presents the analysis of a 3-D tetrahedron formation. The full 3-D rotation of tetrahedron, using a sequence of Euler angles, is presented. The 3-D rotation analysis of a tetrahedron becomes quite complex and is reduced to a 2 angle rotation for simpler analysis. The results for 2-D rotation are presented for different values of the third angle, . It is observed that for a tetrahedron formation only a unique set of charged products exist.

The analysis of the linear 4-craft formation is presented to serve as an open question. A linear 4-craft formation has null-space dimension of 3. This thesis discusses the complexity of determining unique spacecraft charges for a linear formation. The future work in this field should involve determining a method to compute individual charges for formations with null-space dimension higher than 1.

The GA's are the modern tools available to solve optimization problem. Typical gradient based optimization techniques available require a good initial guess to the problem. Also the gradient based methods restrict the search space, for determining a solution, to a local region around the initial guess. The GA's avoid these hurdles and are a useful tool for aerospace based applications.

A drawback of using the GA's is the large amount of computation time required to arrive at a potential solution. The thesis presents the use of a distributed GA as a numerical tool for finding solutions to static Coulomb formation. The implementation of the distributed GA is presented in the thesis. The performance of the distributed GA over several nodes is explored, and results presented for run time of the GA.

The static formation solutions determined by the distributed GA has open loop charged solution. There is no feedback of charges to maintain the static Coulomb formation. Future work could potentially involve computing the spacecraft charges required to maintain the static formation. The stability of the static formations is also an area of research that needs to be explored.

Bibliography

[1] J. Bristow, D. Folta, and K. Hartman, "A Formation Flying Technology Vision," *AIAA 2000 Space Conference and Exposition*, Long Beach, CA, September 19-21 2000. Paper No. AIAA 2000-5194.

[2] M. Xin, S. Balakrishnan, and H. Pernicka, "Position and Attitude Control of Deep-Space Spacecraft Formation Flying via Virtual Structure and $\theta - D$ Technique," *AIAA Guidance Navigation and Control Conference and Exhibit*, San Francisco, CA, August 15-18 2005. Paper No. AIAA 2000-6090.

[3] P. Gurfil and N. Kasdin, "Dynamics and Control of Spacecraft Formation Flying in Three Body Trajectories," *AIAA Guidance Navigation and Control Conference and Exhibit*, Montreal, Canada, August 6-9 2001. Paper No. AIAA 2001-4026.

[4] J. Leitner, F. Bauer, D. Folta, M. Moreau, R. Carepenter, and J. How, "Formation Flight in Space: Distributed Spacecraft Systems Develop New GPS Capabilities," *GPS World*, Feb 2001.

[5] L. King, G. Parker, and S. Deshmukh, "Spacecraft Formation Flying using Inter-Vehicle Coulomb Forces," tech. rep., NASA/NIAC, January 2002.

[6] L. King, G. Parker, and S. Deshmukh, "Study of Interspacecraft Coulomb Forces and Implication for Formation Flying," *AIAA Journal of Propulsion and Power*, Vol. 19, No. 3, May-June 2003.

[7] J. Berryman and H. Schaub, "Analytical Charge Analysis for 2- and 3-Craft Coulomb Formations," *AAS/AIAA Astrodynamics Specialist Conference*, Lake Tahoe, CA, August 7–11 2005. Paper No. AAS 05–278.

[8] V. Coverstone-Carroll, "Near-Optimal Low-Thrust Trajectories Via Micro-Genetic Algorithms," *Journal of Guidance, Control, and Dynamics*, Vol. 20, No. 1, 1997.

[9] K. KrishnaKumar, "Genetic algorithms - An introduction and an overview of their capabilities," *AIAA Guidance,Navigation and Control Conference*, Hilton Head Island, SC, Aug. 10–12 1992. Paper No. AIAA-1992-4462.

[10] F. Peng, Y.-R. Hu, and A. Ng, "Testing of Membrane Space Structure Shape Control Using Genetic Algorithm," *Journal of Spacecraft and Rockets*, Vol. 43, No. 4, 2006.

[11] W. Yi, Q. Liu, and Y. He, "Dynamic distributed genetic algorithms," *Proceedings of the 2000 Congress on Evolutionary Computation*, Vol. 2, 2000.

[12] J. Berryman and H. Schaub, "Static Equilibrium Configurations in GEO Coulomb Spacecraft Formations," *AAS Spaceflight Mechanics Meeting*, Copper Mountain, CO, Jan. 23–27 2005. Paper No. AAS 05–104.

[13] L. Pettazzi, H. Kruger, and S. Theil, "Electrostatic forces for satellite swarm navigation and reconfiguration," tech. rep., ESA, January 2006.

[14] A. Natarajan, H. Schaub, and G. G. Parker, "Reconfiguration of a 2-Craft Coulomb Tether," *AAS Space Flight Mechanics Meeting*, Tampa, FL, Jan. 22–26 2006. Paper No. AAS-06-229.

[15] H. Schaub, C. D. Hall, and J. Berryman, "Necessary Conditions for Circularly-Restricted Static Coulomb Formations," *AAS Malcolm D. Shuster Astronautics Symposium*, Buffalo, NY, June. 12–15 2005. Paper No. AAS 05–472.

[16] H. Schaub and M. Kim, "Orbit Element Difference Constraints for Coulomb Satellite Formations," *AIAA/AAS Astrodynamics Specialist Conference*, Providence, Rhode Island, Aug. 2004. Paper No. AIAA 04-5213.

[17] S. Wang and H. Schaub, "Spacecraft Collision Avoidance Using Coulomb Forces With Separation Distance Feedback," *AAS Space Flight Mechanics Meeting*, Sedona, AZ, Jan. 28–Feb. 1 2007. Paper AAS 07–112.

[18] L.Pettazzi, D.Izzo, and S.Theil, "Swarm Navigation and Reconfiguration using Electrostatic Forces," *7th International Conference on Dynamics and Control of Systems and Structures in Space*, Greenwich, London, England, July 19–20 2006.

[19] D. Izzo and L. Pettazzi, "Self-assembly of large structures in Space using inter-satellite Coulomb forces," *56th International Astronautical Congress*, Fukuoka, Japan, Oct. 17-21 2005.

[20] M. A. Peck, "Prospects and Challenges for Lorentz-Augmented Orbits," *AIAA Guidance, Navigation and Control Conference*, San Francisco, CA, August 15–18 2005. Paper No. AIAA 2005-5995.

[21] J. Atchison, B. Streetman, and M. Peck, "Prospects for Lorentz Augmentation for Jovian Captures," *AIAA Guidance, Navigation and Control Conference and Exhibit*, Keystone,Colorado, August 21–24 2006.

[22] U. Ahsun, "Dynamics and Control of Electromagnetic Satellite Formations in Low Earth Orbits," *AIAA Guidance, Navigation and Control Conference and Exhibit*, Keystone,Colorado, August 21–24 2006.

[23] E. M. Kong and D. W. K. et.al, "Electromagnetic Formation Flight for Multisatellite Arrays," *Journal of Spacecraft and Rockets*, Vol. 41, No. 4, 2004.

[24] H. Schaub and J. L. Junkins, *Analytical Mechanics of Space Systems.* Reston, VA: AIAA Education Series, October 2003.

[25] W. Clohessy and R. Wiltshire, "Terminal Guidance System for Satellite Rendezvous," *Journal of the Aerospace Sciences*, Vol. 27, No. 9, September 1960.

[26] G. W. Hill, "Researches in Lunar Theory," *American Journal of Mathematics*, Vol. 1, No. 1, 1878.

[27] S. Wang and H. Schaub, "One-Dimensional 3-Craft Coulomb Structure Control," *7th International Conference on Dynamics and Control of Systems and Structures in Space*, Greenwich, London, England, July 19–20 2006, pp. 269–278.

[28] J. Berryman, "Analytical and Numerical Analysis of Static Coulomb Formations," Master's thesis, Virginia Tech, 2005.

Appendix A

Appendix

Table A.1 lists the positions and charges of the tetrahedron presented in figure 3.9

Table A.1: Positions and Charges on a Tetrahedron formation

Spacecraft pos.	x_i $[m]$	y_i $[m]$	z_i $[m]$	$\tilde{q}_i$ $[C\frac{\sqrt{k}}{n}]$
1	0	-15	0	0
2	4.1793	5	-13.5105	622.5133
3	9.6108	5	10.3746	2051.3499
4	-13.7901	5	3.1359	-1027.2352

Table A.2 lists the positions and charges of the spacecraft formations found using distributed GA and presented in figure 4.8

Table A.2: Positions and Charges on Coulomb Virtual Structures

Description	Spacecraft pos.	x_i $[m]$	y_i $[m]$	z_i $[m]$	$\tilde{q}_i$ $[C\frac{\sqrt{k}}{n}]$
4-Spacecraft Formation	1	2.054699	-19.194995	0.029969	-376.794771
	2	4.546227	-2.469598	-0.058823	-290.354447
	3	-15.815114	5.951197	0.002398	2164.473377
	4	9.214187	15.713395	0.026456	-1091.559875
4-Spacecraft Formation	1	-14.436179	9.938727	-1.745685	1754.643272
	2	7.483702	2.568276	12.215681	-697.494363
	3	12.675835	2.862896	-9.595137	-1779.519213
	4	-5.723358	-15.369899	-0.874859	586.077423
5-Spacecraft Formation	1	-10.293449	2.669913	-12.764823	-793.129491
	2	16.955803	2.219767	-6.063810	2900.697698
	3	-1.012350	-9.449045	-0.484354	-36.939263
	4	6.232131	1.902031	11.063759	238.899077
	5	-11.882136	2.657334	8.249228	-1185.213879
6-Spacecraft Formation	1	-2.998938	-11.710008	8.880229	-494.745942
	2	-4.781952	26.120298	-0.048563	-1212.799408
	3	-3.868946	4.951687	0.456478	-266.339279
	4	-3.659234	-11.621703	-9.007252	-663.850296
	5	-0.088834	-11.984687	0.030299	-3.673028
	6	15.397904	4.244412	-0.311192	1613.121742
10-Spacecraft Formation	1	4.267563	-21.013826	1.431670	-525.090023
	2	4.654116	4.366676	1.640141	-419.790237
	3	7.892757	-6.321177	20.144326	-1466.074524
	4	2.507399	4.291338	-5.203640	-88.426301
	5	3.173858	-23.805024	-13.692794	-546.086956
	6	0.234183	-5.254377	-1.171747	20.013245
	7	-27.810947	1.128117	2.587026	3662.144882
	8	-1.704943	-11.902567	0.314594	69.625352
	9	4.561632	28.324227	-12.842382	-1121.388268
	10	2.224383	30.186613	6.792806	-336.376041